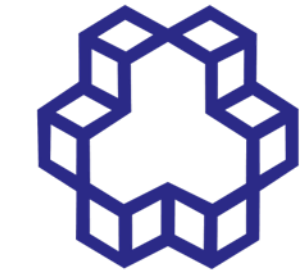

Faculty of Electrical Engineering

Final Project of Robust Control

Design and Analysis of H_∞ and μ-Synthesis-Based Attitude Controllers for a Quadrotor

By

Kosar Aminjafari

Amirhossein Mohammadi

Supervisor

Hamid D. Taghirad

July 2025

Abstract

This study addresses robust attitude control for quadrotor UAVs under modeling uncertainty and actuator constraints. Experimental system identification employed chirp signals from 0.05 to 5 Hz with amplitudes between 5° and 11°, producing reliable pitch and roll models. Design specifications targeted a settling time of approximately 0.3 seconds, 0% overshoot, and control effort within ±20° actuator bounds. Optimized H_∞ controllers achieved gamma values of 0.934 (pitch) and 0.71 (roll) through iterative tuning with sensitivity gain coefficients of 850 and 650, respectively. Monte Carlo simulations confirmed consistent performance across 6 system instances (1 nominal and 5 perturbed), maintaining control signals below ±10° (pitch) and ±7° (roll). Disturbance rejection and sensor noise tests validated robustness, while real-world constraints like actuator saturation were respected. All simulations were conducted in MATLAB and Simulink, with full implementation provided in a reproducible Jupyter Notebook hosted on GitHub.

Keywords: Robust Control, Quadrotor Attitude Control, H_∞ Synthesis, μ-Synthesis

Table of Contents

1. Introduction

The stabilization and precise control of quadrotor unmanned aerial vehicles (UAVs) remain a critical challenge in aerial robotics due to their inherently nonlinear, underactuated dynamics and susceptibility to various uncertainties, such as unmodeled dynamics, external disturbances, and parametric variations. As these platforms continue to gain prominence in applications ranging from search and rescue missions to delivery services and environmental monitoring, the need for robust and high-performance attitude control strategies becomes increasingly imperative.

Conventional control approaches like PID and LQR, while effective in certain operating regimes, often fall short in maintaining stability and performance in the presence of real-world uncertainties and input constraints. To address these limitations, robust control methods such as H_∞ control and μ-synthesis have emerged as powerful tools capable of delivering guaranteed performance and stability margins even under structured or unstructured perturbations.

This report presents the design, implementation, and analysis of attitude controllers for a quadrotor (which is called robot in this report) based on both H_∞ and μ-synthesis frameworks. Using frequency-domain system identification techniques applied to experimental data, nominal linear models for the roll and pitch dynamics are derived along with multiplicative uncertainty bounds. These models serve as the foundation for synthesizing H_∞ controllers that achieve robust stabilization and disturbance rejection while respecting actuator limitations.

The design methodology follows a cascade control architecture, where the robust controller augments an existing inner-loop PID stabilizer. Performance specifications including stringent settling time and minimal

overshoot requirements are integrated via sensitivity and control weighting functions in the mixed-sensitivity formulation.

Overall, the design carried out in this project pursues the following steps and objectives.

- System Identification and Linear Modeling
- Interpreting the System with a Linear and Multiplicative Uncertainty Model
- H_∞ Controller Design to provide Robust Stability and Nominal Performance
- Design Improvement of the H_∞ Controller
- μ-Synthesis-Based Controller Design to provide Robust Stability and Nominal Performance
- Model (Order) Reduction of the μ-Synthesis-Based Controller
- Comparison of the Designed Controllers in the Time and Frequency Domains

When it comes to technical implementation, to facilitate reproducibility and transparency, a single Jupyter Notebook file is attached alongside this report. It contains all of the MATLAB-based technical implementations in the exact order in which they appear throughout the chapters of this report. Using a Notebook instead of multiple .m files enables a more seamless and interactive presentation of code, explanations, and results all in one place enhancing readability, reproducibility, and workflow efficiency.

To further support accessibility and ensure long-term availability of the source code and notebook, the full implementation is also hosted in a public GitHub repository:

https://github.com/AmirhosseinMuhammadi/Robust-Control.

This allows readers to review, reuse, or extend the work with minimal setup.

2. Modeling and System Identification

The first step to design controllers and simulate the dynamic behavior of the system, is to obtain the theoretical model which is basically extracting the differential equations governing the system. These equations are actually the equations of motion that are obtained from Newton's and Euler's second law of motion. Since the report focuses mostly on controller design, here is a brief overview of this section.

2.1. System Introduction

As illustrated in Figure 2.1, the robot possesses six degrees of freedom in which three of them are translational (motion along the x, y, and z axes) and the others are rotational namely roll (ϕ), pitch (θ), and yaw (ψ).

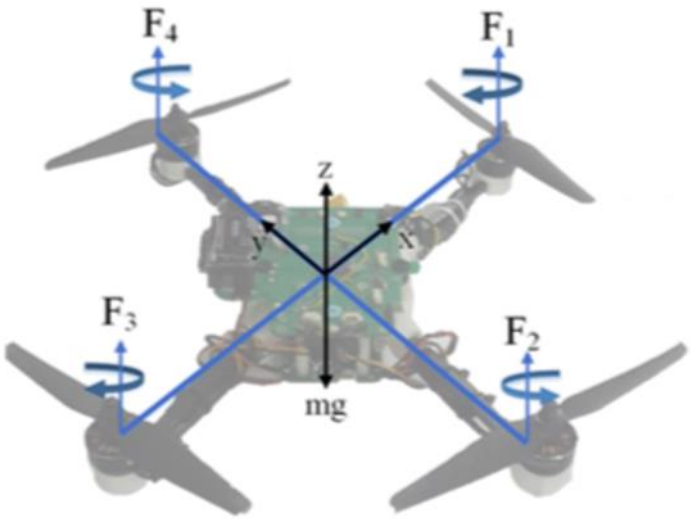

Figure 2.1. Quadrotor Body Frame, Rotor Arrangement and Corresponding Forces

However, the objective of this project is the attitude stabilization, not a full 6-DOF trajectory control. Therefore, the rotational dynamics are modeled because these directly impact flight stability especially during hover and minor maneuvers. The associated non-linear equations of motion governing the robot are as follows.

$$\ddot{\phi} = \frac{J_r \dot{\theta}(\Omega_1 + \Omega_3 - \Omega_2 - \Omega_4)}{I_{xx}} + \frac{I_{yy} - I_{zz}}{I_{xx}} \theta\dot{\psi} + \frac{bl(\Omega_2^2 - \Omega_4^2)}{I_{xx}}$$

(Equation 2.1)

$$\ddot{\theta} = \frac{J_r \dot{\phi}(-\Omega_1 - \Omega_3 + \Omega_2 + \Omega_4)}{I_{yy}} + \frac{I_{zz} - I_{xx}}{I_{yy}} \dot{\phi}\dot{\psi} + \frac{bl(\Omega_3^2 - \Omega_1^2)}{I_{yy}}$$

(Equation 2.2)

$$\ddot{\psi} = \frac{d(\Omega_1^2 + \Omega_3^2 - \Omega_2^2 - \Omega_4^2)}{I_{zz}} + \frac{I_{xx} - I_{yy}}{I_{zz}} \dot{\phi}\dot{\theta}$$

(Equation 2.3)

Table 2.1 shows the symbols used in the equations.

Table 2.1. List of Symbols in Equations of Motion

Symbol	Description
$I_{xx, yy, zz}$	Inertia Moments
J_r	Rotor Inertia
Ω_i	Propeller Angular Rate
D	Drag Factor
B	Trust Factor
l	Horizontal Distance: Propeller Center to CoG

2.1.1. Determination of the Nominal Models

In the reviewed paper, the robot is considered as a black-box and experimental data are collected. Chirp signals with varying frequencies 0.05–5 Hz and amplitudes of 5–11° are injected as reference inputs and a PID controller is used to maintain stability during these tests as shown in Figure 2.2. The selected values are within the response range of the robot.

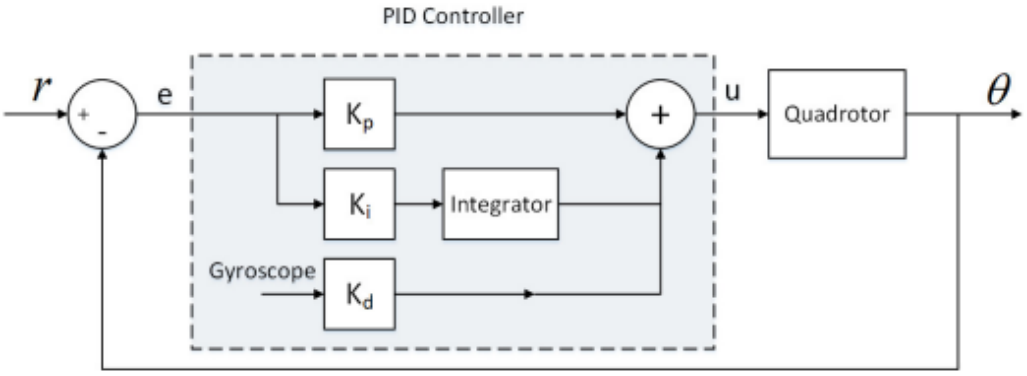

Figure 2.2.PID Controller for the Robot

Experiments are conducted independently for roll and pitch channels to reduce cross-axis coupling and simplify identification. This approach results in two distinct Single- Input Single-Output (SISO) subsystems, one governing the pitch dynamics and the other governing the roll. However, a quadrotor is inherently a Multiple Input Multiple-Output (MIMO) system. Therefore, the following can be stated to justify this method.

- Practical Constraints: Open-loop instability made MIMO Identification challenging.
- According to the reference paper and Figures 2.3 and 2.4 coupling effects were small near hover conditions.
- The coupling effects can be considered as a part of the uncertainties.

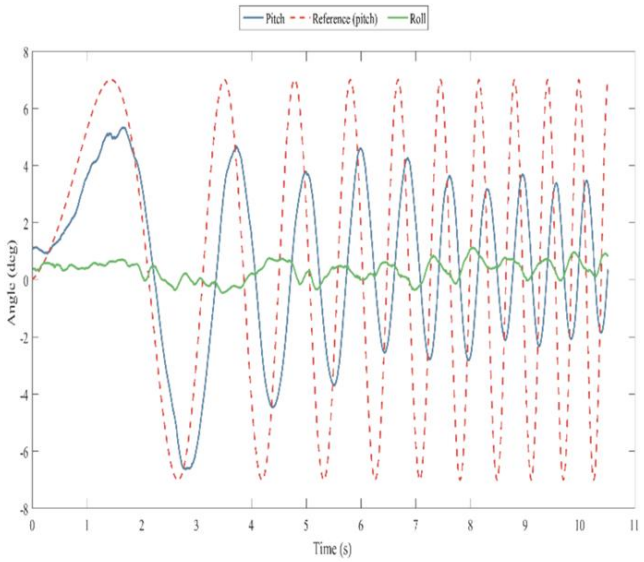

Figure 2.3. Coupling Effect of the Pitch on the Roll

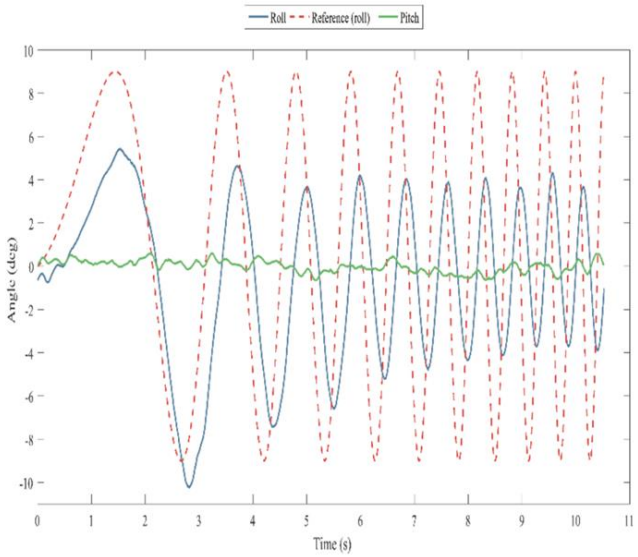

Figure 2.4. Coupling effect of the roll on the pitch

For each dataset (8 for pitch, 9 for roll), 15 different transfer functions are fit using MATLAB's CONTSID toolbox and models with three poles and no zeros are generally selected as best representations due to good frequency-domain consistency and physical plausibility.

Figures 2.5 and 2.6 show the Bode diagrams of the transfer functions obtained for the pitch and roll angles. It can be seen that the behavior of the transfer functions is similar, especially in frequencies less than 15Hz where the robot mostly operates in.

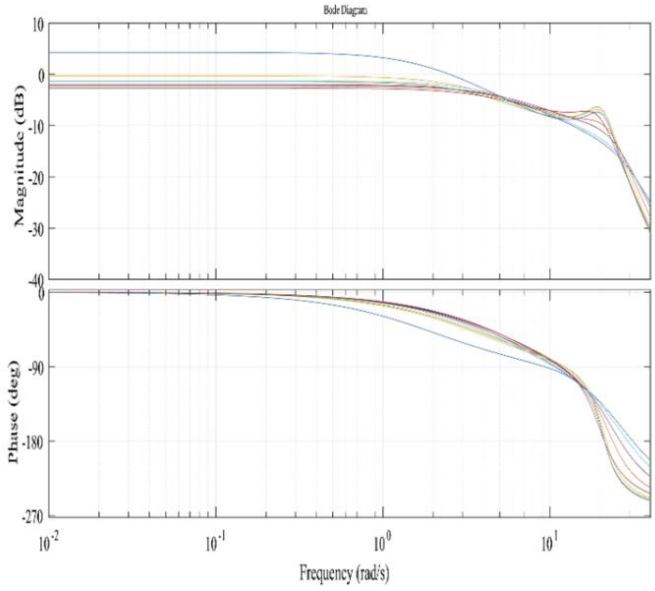

Figure 2.5. Bode diagram of selected transfer functions in the experiments (Pitch)

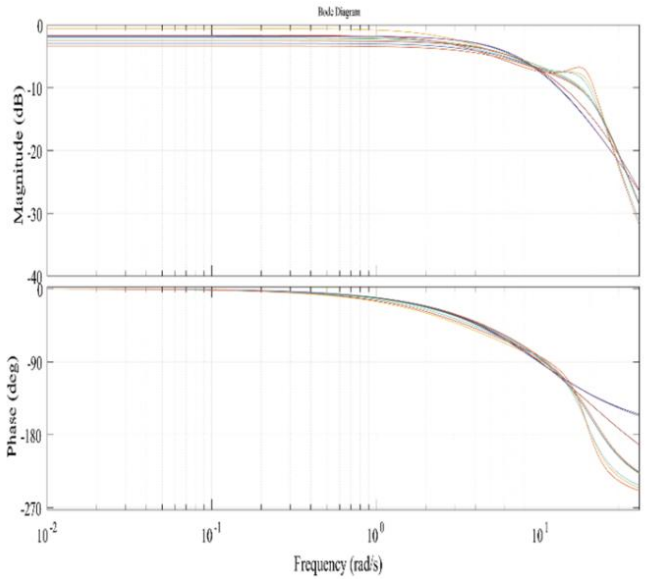

Figure 2.6. Bode diagram of selected transfer functions in the experiments (Roll)

Finally, the transfer functions closest to the median Bode response across experiments are selected as the nominal models and are as follows.

$$G_\theta(s) = \frac{1547.4}{(s+5.373)(s^2+10.12s+390.4)} \textit{ (Equation 2.4)}$$

$$G_\phi(s) = \frac{2049.8}{(s+6.764)(s^2+19.03s+426.2)} \textit{ (Equation 2.5)}$$

2.1.2. Uncertainty Estimation

In many dynamic systems, uncertainty is introduced due to factors such as high-frequency perturbations and unmodeled dynamics. To represent these uncertainties, an unstructured multiplicative perturbation model is commonly utilized. In this framework, the family of uncertain systems is expressed as follows.

$$G_p(s) = (1 + \Delta W)G_0(s) \textit{ (Equation 2.6)}$$

Where $G_0(s)$ denotes the nominal transfer function, $W(s)$ is a weighting function characterizing the uncertainty profile, and $\Delta(s)$ represents a stable perturbation satisfying $||\Delta||_\infty < 1$.

This modeling approach allows both parametric and structural uncertainties to be encapsulated within a single full-block representation. For

robust control design, an approximate linear model along with an appropriately chosen weighting function is typically required.

In order to estimate the associated weighting functions, other fitted models are treated as perturbations around the nominal and a weighting function *W(s)* is fitted as an upper bound over these deviations. The final weighting functions are as follows.

$$W_\theta(s) = \frac{1659.6(s^2+2.868s+60.44)}{(s+9.678)(s+24770)} \textit{ (Equation 2.7)}$$

$$W_\phi(s) = \frac{1.9017(s^2+3.813s+91.61)}{s^2+43.53s+545.3} \textit{ (Equation 2.8)}$$

2.1.3. Control Problem Structure

As mentioned, the cascade architecture can be used for MIMO systems, uncertainty reduction and design improvements. Inside the inner loop a basic PID is used during system identification to stabilize the robot and collect experimental data. This PID is crude but sufficient for safe hovering during data collection. On the other hand, the outer loop contains the H_∞ controller that is designed based on the identified closed-loop model (which includes the effects of the PID) and it augments it in a cascade architecture as shown in Figure 2.7.

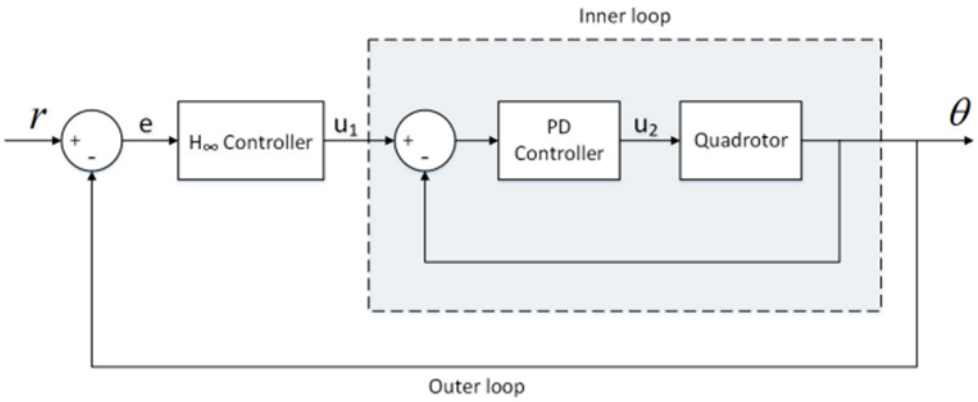

Figure 2.7. Control Structure (Block Diagram)

2.2. Modeling Uncertain SISO Systems

The derived transfer functions are implemented in MATLAB (refer to the attached notebook) using the ultidyn function to model uncertain elements, enabling probabilistic sampling and analysis. This approach generates perturbed systems for both pitch and roll channels with multiplicative uncertainty, as demonstrated in the accompanying code.

2.3. Uncertainty Visualization

Bode plots comparing the nominal and perturbed system responses are generated using 10 random samples from the uncertain models. While similar analyses were presented earlier, Figures 2.5 and 2.6 are included here for completeness. Note that Figures 2.8 and 2.9 display the nominal and perturbed systems after MATLAB modeling, whereas earlier figures (e.g., 2.5–2.6) were used for identification. As such, minor discrepancies between the results are expected.

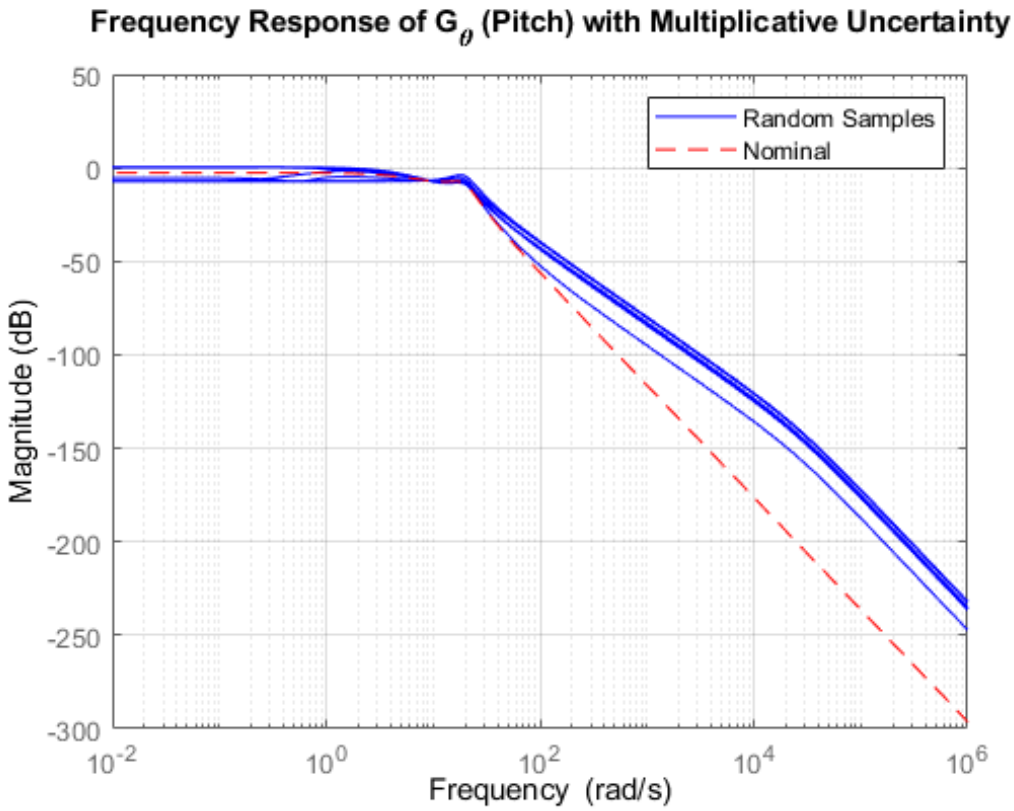

Figure 2.8. Frequency Response of the System with Multiplicative Uncertainty (Pitch)

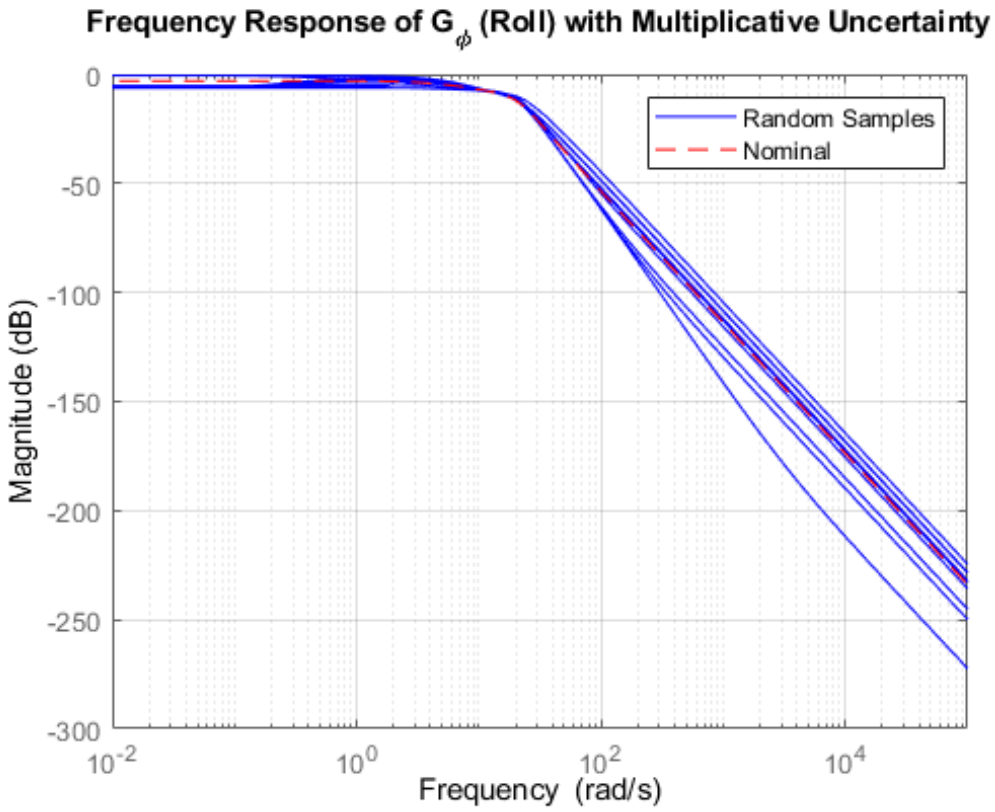

Figure 2.9. Frequency Response of the System with Multiplicative Uncertainty (Roll)

Magnitude bounds (1 ± |W|) illustrate frequency-dependent uncertainty, providing crucial insight for controller synthesis. Figures 2.10 and 2.11 show nominal models along with the upper and lower bounds of the uncertainties that represent the range within which the perturbed frequency response of the system may vary. The upper bound indicates the possible peak magnitude due to uncertainty and the lower bound reflects the minimum expected magnitude under worst-case attenuation.

These bounds facilitate the visualization of the system's robustness to modeling inaccuracies and environmental variability, particularly in the design of controllers that must operate effectively across the entire performance envelope.

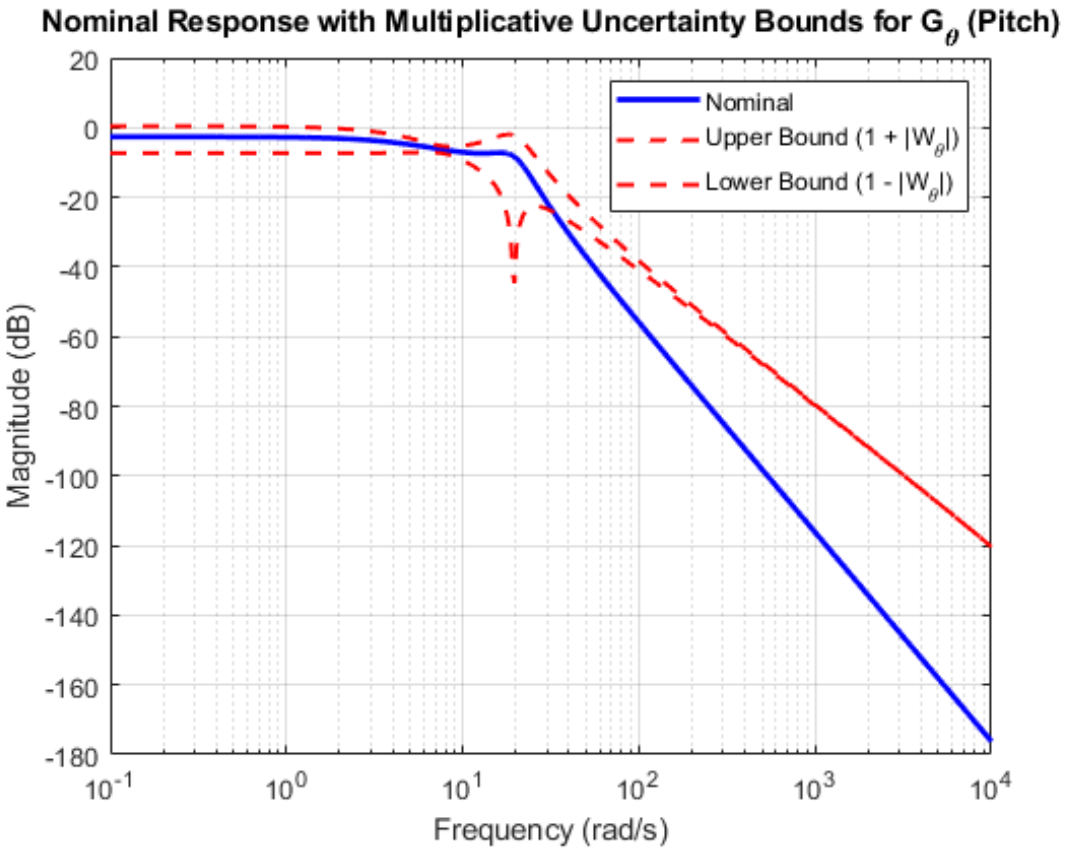

Figure 2.10. Nominal Response with Multiplicative Uncertainty Bounds of the System (Pitch)

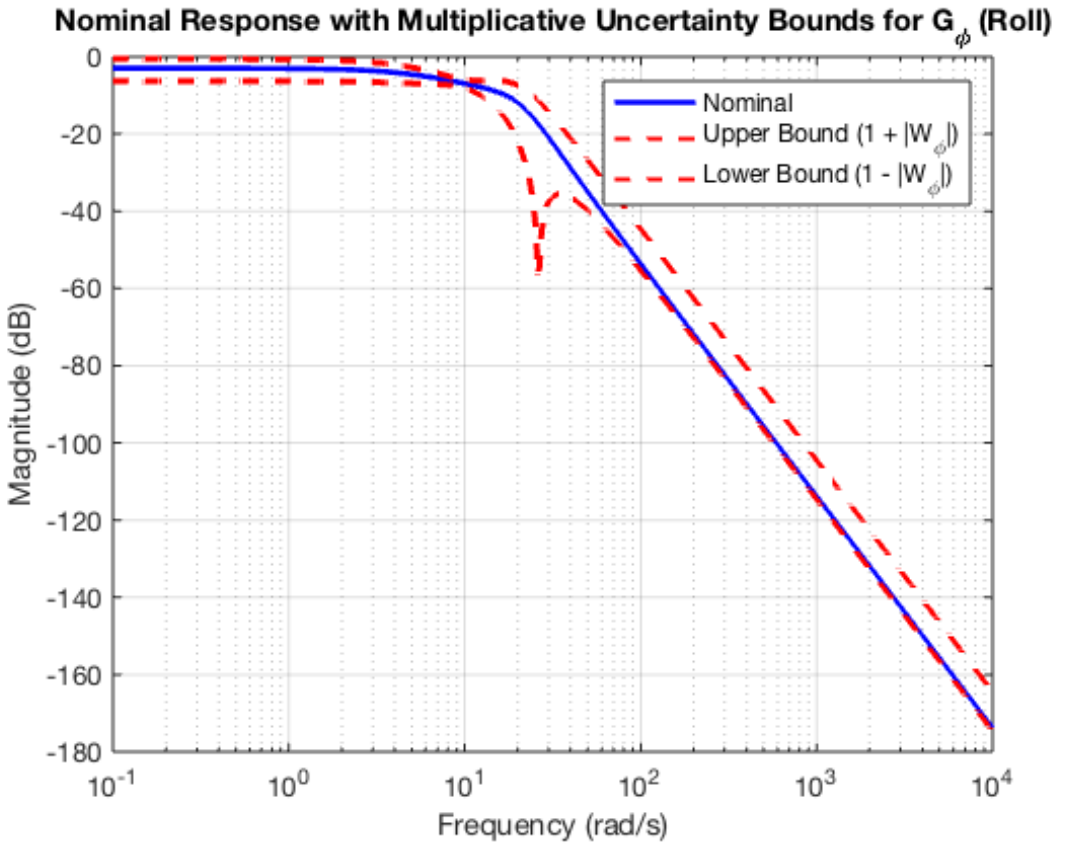

Figure 2.11. Nominal Response with Multiplicative Uncertainty Bounds of the System (Roll)

2.4. Control Objectives and Performance Specifications

Requirements and design criteria are clearly defined in the following.

- Settling time ≈ 0.3 s
- Overshoot ≈ 0%
- Steady-state error ≈ 0
- Control effort within actuator bounds: According to Figure 2.7, the targeted control effort (u_1) is the reference input of the inner loop in the cascade structure. Therefore, it's physically the desired angle (Pitch or Roll) and considered to be less than 20 degrees.

These specifications motivate the design of robust controllers tuned for both performance and actuator feasibility.

3. Robust H_∞ Control Synthesis

The objective of this section is to achieve a controller that provides adequate performance in the presence of mentioned performance constraints while ensuring robust stability in the system. For this purpose, the mixed sensitivity problem needs to be solved.

$$\|T_{wz}\|_\infty = \left\| \begin{matrix} W_s S \\ W_u U \\ WT \end{matrix} \right\|_\infty = \gamma < 1 \text{ (Equation 3.1)}$$

3.1. Sensitivity (Performance) Weighting Function

The sensitivity weighting function $W_s(s)$ is derived from an ideal closed-loop transfer function of a second-order system based on desired settling time and minimal overshoot. Solving peak overshoot criterion leads to the following results.

$$M_\mathrm{p} = \exp\left(-\frac{\pi\zeta}{\sqrt{1-\zeta^2}}\right) \approx 10^{-6} \Rightarrow \zeta = -\frac{\ln(M_p)}{\sqrt{\pi^2+(\ln(M_p))^2}} \Longrightarrow \zeta = 0.975$$

(Equation 3.2)

Where M_p is the peak overshoot and ζ is the required damping ratio.

Having the required damping ratio, the natural frequency is obtained from settling time criterion as follows.

$$T_s \approx \frac{4}{\zeta \omega_n} \approx 0.3s \implies \omega_n = 13.61 \frac{rad}{s} \text{ (Equation 3.3)}$$

In the next step, the ideal closed-loop transfer function can be calculated using the obtained values.

$$T_{id}(s) = \frac{\omega_n^2}{s^2 + 2\zeta\omega_n s + \omega_n^2} = \frac{185.23}{s^2 + 26.68s + 185.23} \text{ (Equation 3.4)}$$

The sensitivity weighting function is obtained as follows according to the mixed sensitivity problem.

$$W_s = a\frac{1}{S_{id}(s)} = a\frac{1}{1 - T_{id}(s)} = \frac{s^2 + 26.68s + 185.23}{s(s + 26.68)} \text{ (Equation 3.5)}$$

Finally, the pole at the origin is moved slightly and also a stable pole far from the origin is added in order to make the weighting function strictly proper and stable.

$$W_s = \frac{s^2 + 26.68s + 185.23}{(s + 0.001)(s + 26.68)(s + 1000)} \text{ (Equation 3.6)}$$

3.2. Control Effort Weighting Function

In order to limit the control effort signal, an appropriate weighting function can be chosen. The actuator itself has a saturation limit of 20° which can be the basis for calculation.

$$\|W_u U\|_\infty \leq 1;\ \|U\|_\infty \leq 20° \implies W_u = 0.05 \text{ (Equation 3.7)}$$

However, the control effort weight is initially set to $W_u = 1$ and could be refined through iterative tuning.

3.3. H_∞ Control Synthesis using Riccati-Based Optimization Method

Using the augmented plants and hinfsyn in MATLAB, structured controllers are synthesized. Resulting gamma value in the initial trial is 1.42 which is more than the allowable value of 1 and is not acceptable.

Figures 3.1 and 3.2 show that the nominal systems do not follow the final value of the unit step input. It can also be seen that the system response is seriously slow and could never be acceptable. There is also an unacceptable overshoot for the control effort signal.

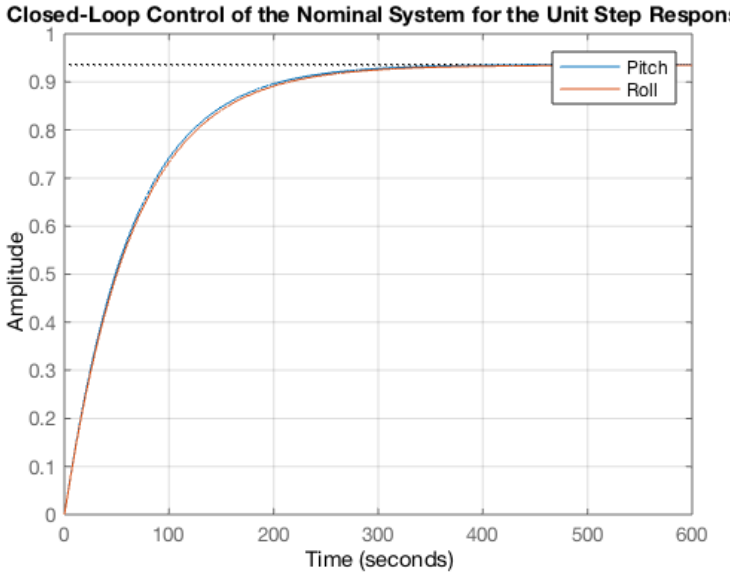

Figure 3.1. Closed-Loop Control of the Nominal Systems for the Unit Step Response

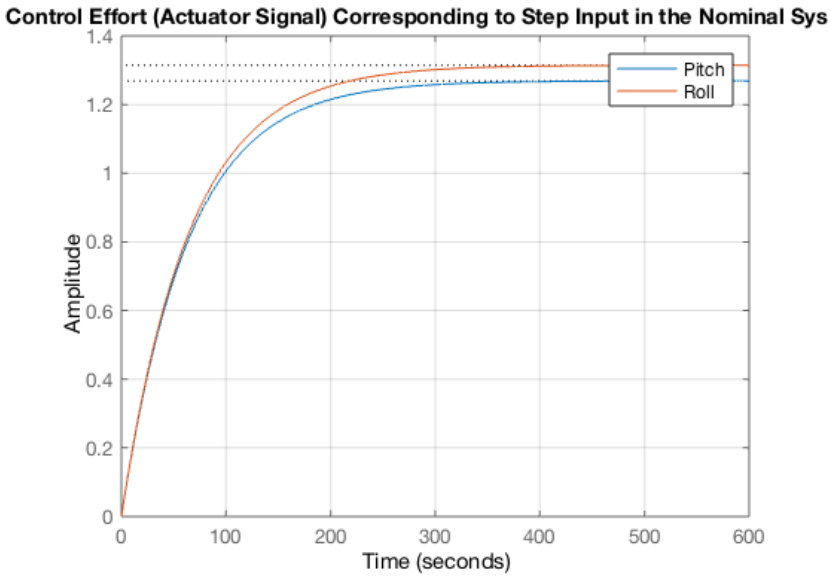

Figure 3.2. Control Effort (Actuator Signal) Corresponding to Step Input in the Nominal Systems

In Figures 3.3 and 3.4 the Bode diagram and singular values are plotted. In addition to the unacceptable maximum singular value, the corresponding curve is not flat in any frequency range and is far from the acceptable curve.

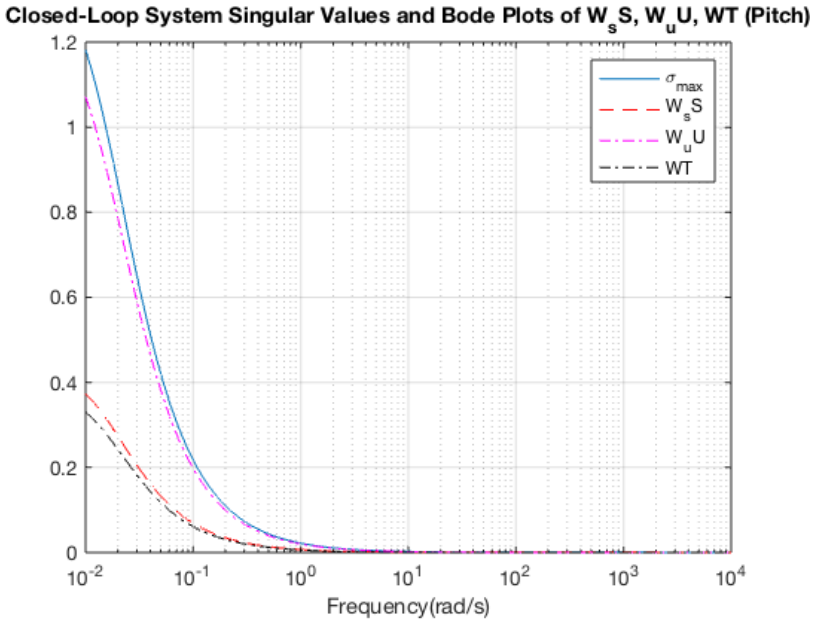

Figure 3.3. Closed-Loop System Singular Values and Bode Plots (Pitch)

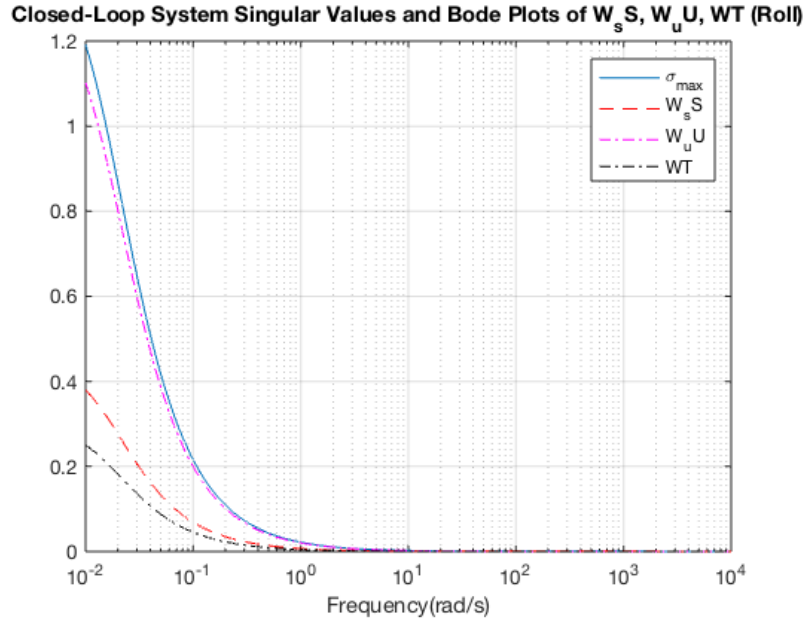

Figure 3.4. Closed-Loop System Singular Values and Bode Plots (Roll)

3.4. Improvement Cycle

Since the control effort signal is far from saturation in Figure 3.2, the constraint condition on it can be relaxed. Therefore, selecting a lower value for W_u shifts the focus of the optimization algorithm more toward performance and sensitivity, while imposing stricter constraints on it due to its poor condition. Based on the actuator saturation and according to Equation 3.7, the control effort weighting function can be fixed with the value of 0.05.

By increasing sensitivity gain coefficient a, controllers are refined through looped simulations. The stepinfo function in MATLAB tracks specification attributes such as settling time, used as feedback to adjust parameters dynamically until desired specs are met. A more detailed iterative process is accessible in the attached Notebook. The optimized objective values are expressed in Table 3.1.

Table 3.1. The Optimized Objective Values

Objective Value	Pitch	Roll
a	850	650
γ (σ_{max})	0.934	0.71

Resulting γ values lie within acceptable bounds, validating stability and performance. The corresponding optimized curves are as follows. It can be seen in Figures 3.5 and 3.6 that the maximum singular value is less than 1 for both control systems and its curve is flat in a large frequency range. It is also observed that the control effort constraint in this design is much weaker and the main contribution to the maximum singular value is created by the performance transfer function.

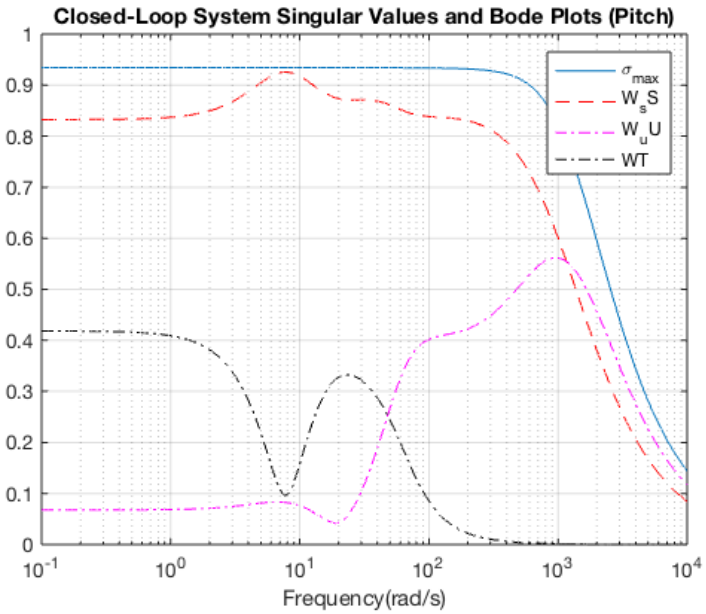

Figure 3.5. Improved Closed-Loop System Singular Values and Bode Plots (Pitch)

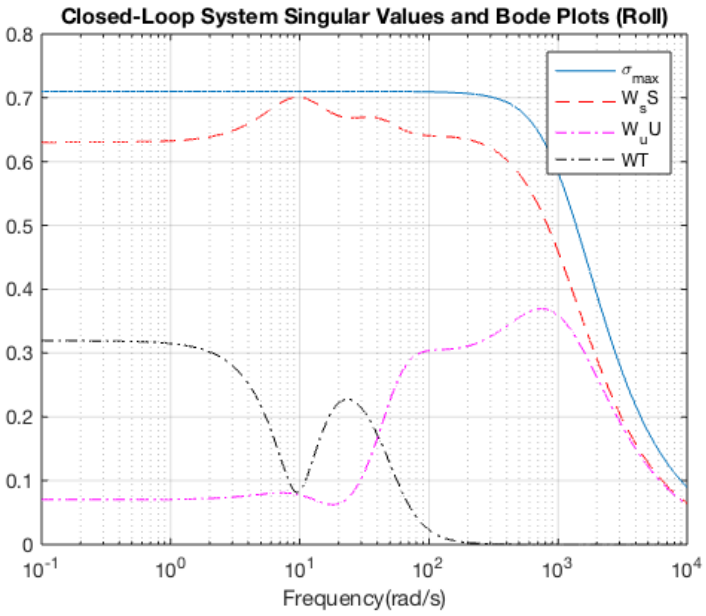

Figure 3.6. Improved Closed-Loop System Singular Values and Bode Plots (Roll)

The controllers also satisfy design objectives. Step responses of nominal closed-loop systems show smooth, fast and almost critically damped behavior as shown in Figures 3.7 and 3.8.

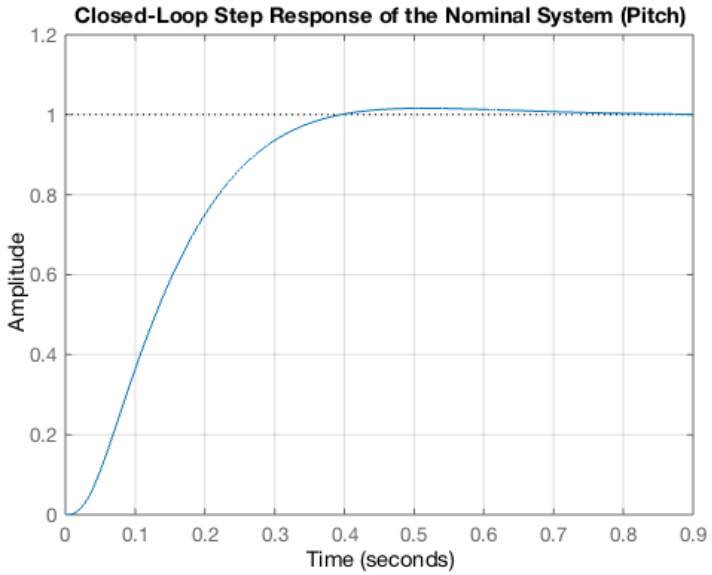

Figure 3.7. Improved Closed-Loop Pitch Control of the Nominal Systems for the Unit Step Response

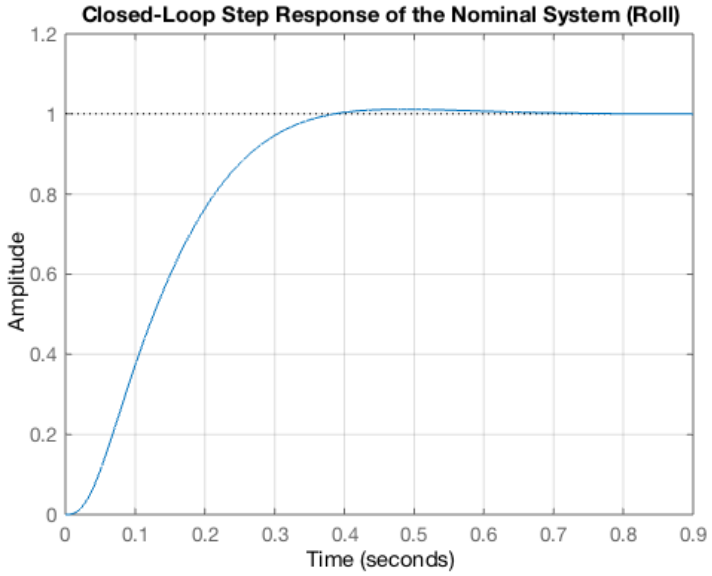

Figure 3.8. Improved Closed-Loop Roll Control of the Nominal Systems for the Unit Step Response

Control signals are within the specified saturation limits of ±20°, confirming that the synthesized controllers respect actuator constraints under nominal operating conditions. As visualized in Figures 3.9 and 3.10, the control inputs remain well-behaved, showing smooth transient behavior without excessive peaks or sharp discontinuities. This reinforces the effectiveness of the weighting function design in shaping control effort and

validates that the closed-loop system remains physically realizable across its operating envelope.

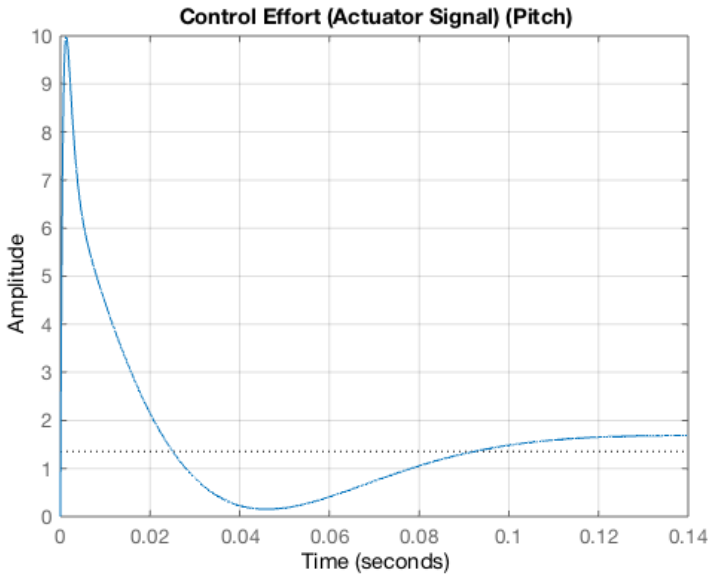

Figure 3.9. Control Effort (Actuator Signal) Corresponding to Step Input in the Improved Nominal System (Pitch)

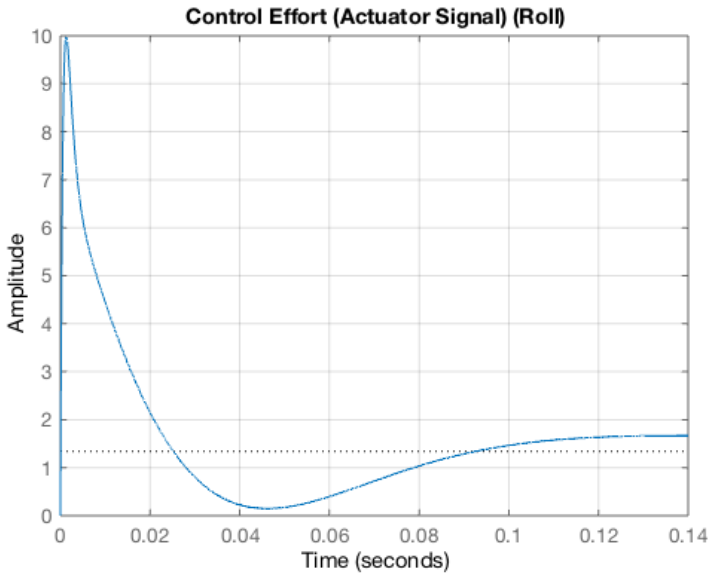

Figure 3.10. Control Effort (Actuator Signal) Corresponding to Step Input in the Improved Nominal System (Roll)

3.5. Robustness Against Uncertainty

The derived optimal robust H_∞ controllers for pitch and roll angles are 8th-order rational transfer functions as expressed in Equations 3.8 and 3.9.

$$C_\theta(s) = \frac{2.369\times10^4\, s^7 + 5.982\times10^8\, s^6 + 2.858\times10^{11}\, s^5 + 1.872\times10^{13}\, s^4 + 4.554\times10^{14}\, s^3 + 8.612\times10^{15}\, s^2 + 7.941\times10^{16}\, s + 2.344\times10^{17}}{s^8 + 2.715\times10^4 s^7 + 6.056\times10^7 s^6 + 3.819\times10^{10} s^5 + 3.997\times10^{12} s^4 + 2.165\times10^{14} s^3 + 4.539\times10^{15} s^2 + 2.44\times10^{16} s + 2.44\times10^{13}}$$

(Equation 3.8)

$$C_\phi = \frac{1.258\times10^4 s^7 + 6.534\times10^6 s^6 + 6.665\times10^8 s^5 + 3.016\times10^{10} s^4 + 7.851\times10^{11} s^3 + 1.256\times10^{13} s^2 + 1.142\times10^{14} s + 3.868\times10^{14}}{s^8 + 2032\, s^7 + 1.172\times10^6 s^6 + 1.496\times10^8 s^5 + 9.86\times10^9 s^4 + 3.484\times10^{11} s^3 + 5.991\times10^{12} s^2 + 3.843\times10^{13} s + 3.843\times10^{10}}$$

(Equation 3.9)

- Pitch Controller $C_\theta(s)$: High-order polynomial ensuring sharp transient control
- Roll Controller $C_\phi(s)$: Similarly structured for balanced performance

Monte Carlo simulations were conducted using the usample function on a total of 6 system instances 1 nominal model and 5 randomly perturbed models derived from the structured uncertainty definitions. For each case, step responses of the closed-loop system and corresponding control signals were evaluated.

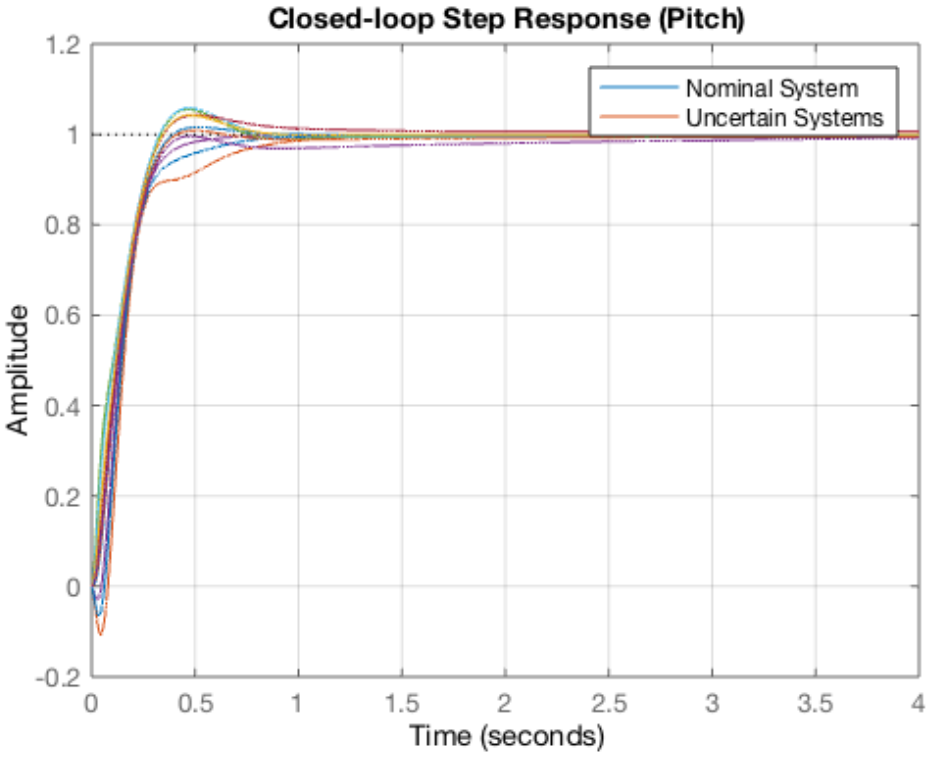

Figure 3.11. Closed-Loop Step Response of Uncertain Systems (Pitch)

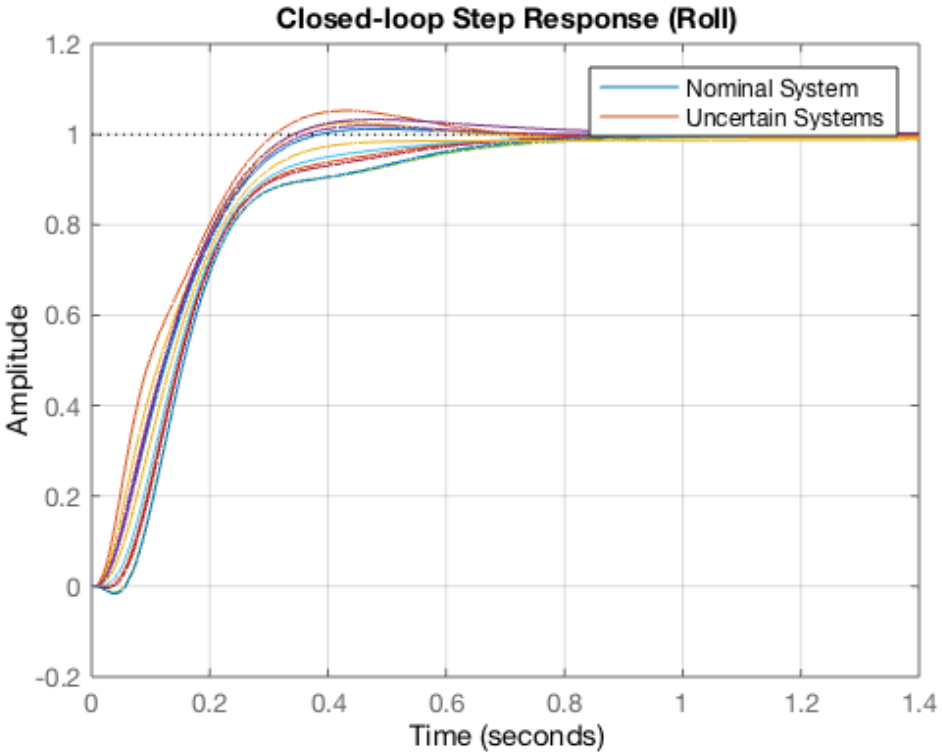

Figure 3.12. Closed-Loop Step Response of Uncertain Systems (Roll)

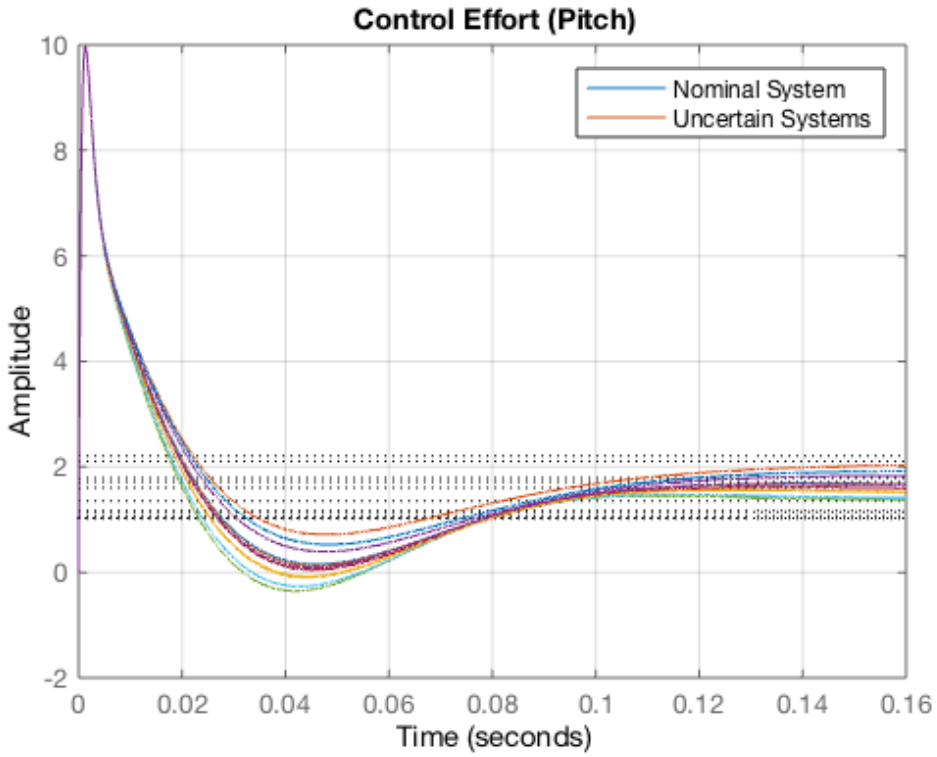

Figure 3.13. Control Effort Corresponding to Step Input in the Uncertain Systems (Pitch)

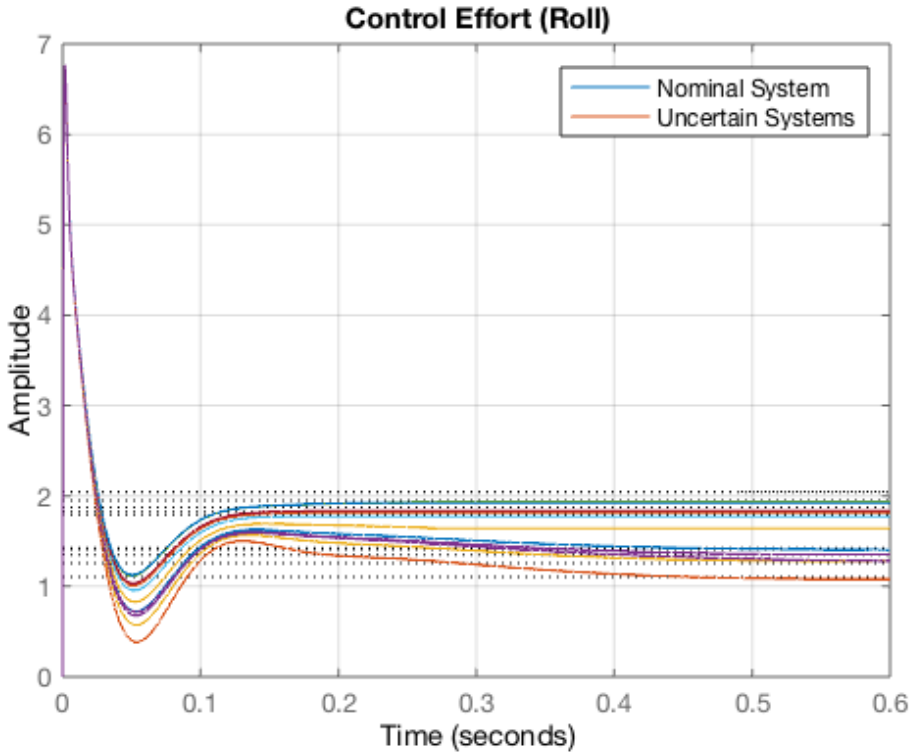

Figure 3.14. Control Effort Corresponding to Step Input in the Uncertain Systems (Roll)

The results demonstrate consistent transient behavior across all simulations, with maximum control efforts staying within ±10° for pitch and ±7° for roll. Despite variation in system dynamics due to uncertainty, the controllers ensured settling times below 1 second and minimal overshoot (<2%) in all instances. This validates the robustness of the synthesized controllers and confirms their suitability under realistic conditions where parameter deviations and modeling errors are present.

3.6. Real-World Constraints: Actuator Saturation

Actuator saturation refers to the physical limits of the actuators in a system (motors, valves, etc.). Every real-world actuator has:

- Upper limit: Maximum force/voltage/speed it can provide
- Lower limit: Minimum value (often zero, but could be negative for bidirectional actuators)

When the controller demands values beyond these limits, the actuator saturates (can't deliver more).

However, as mentioned in the previous chapters the control effort under review is actually the reference input of the inner loop in the cascade architecture. Therefore, it's physically the desired angle (pitch or roll) and considered to be less than 20°.

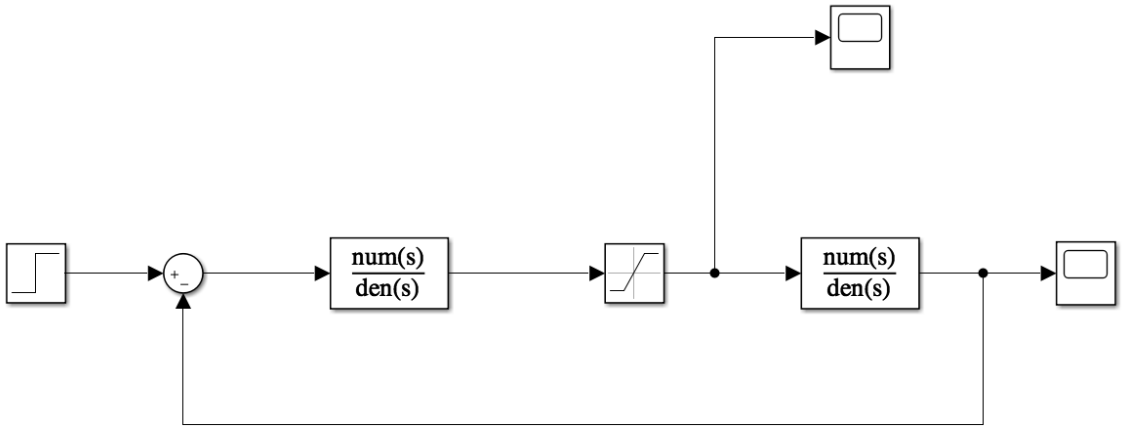

Figure 3.15. Simulation using Simulink in the Presence of Saturation

Simulation is done using Simulink with the presence of saturation block and the resulting curves are as follows.

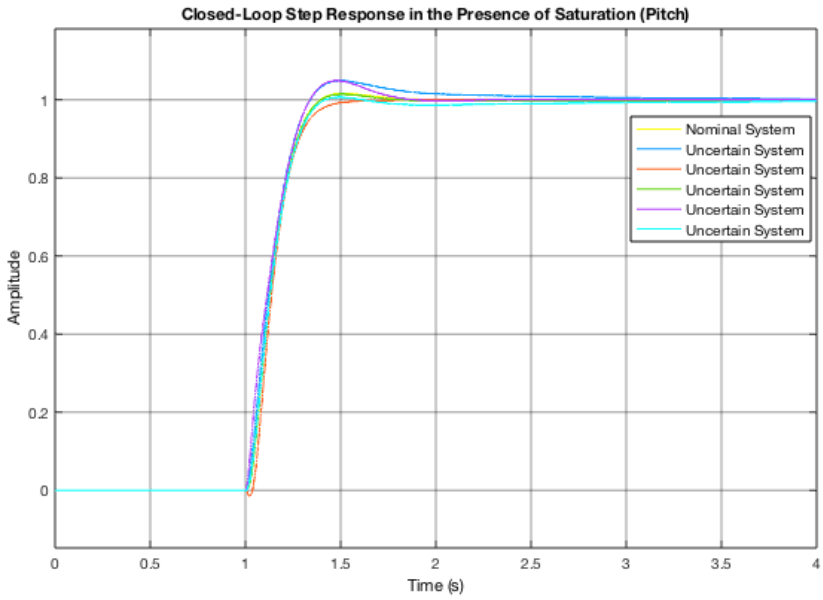

Figure 3.16. Closed-Loop Step Response in the Presence of Saturation (Pitch)

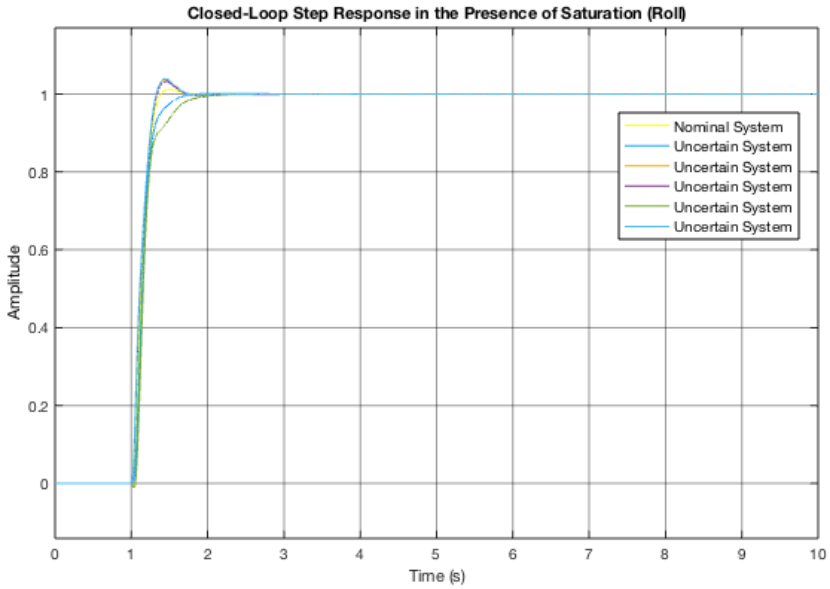

Figure 3.17. Closed-Loop Step Response in the Presence of Saturation (Roll)

Since the controller output is a reference for inner-loop PID (i.e., desired pitch/roll angles), signals must stay below ±20 degrees. Simulations confirm this, preserving safe operational bounds. It can be concluded from Figures 3.16-3.19 that no changes are observed compared to previous curves.

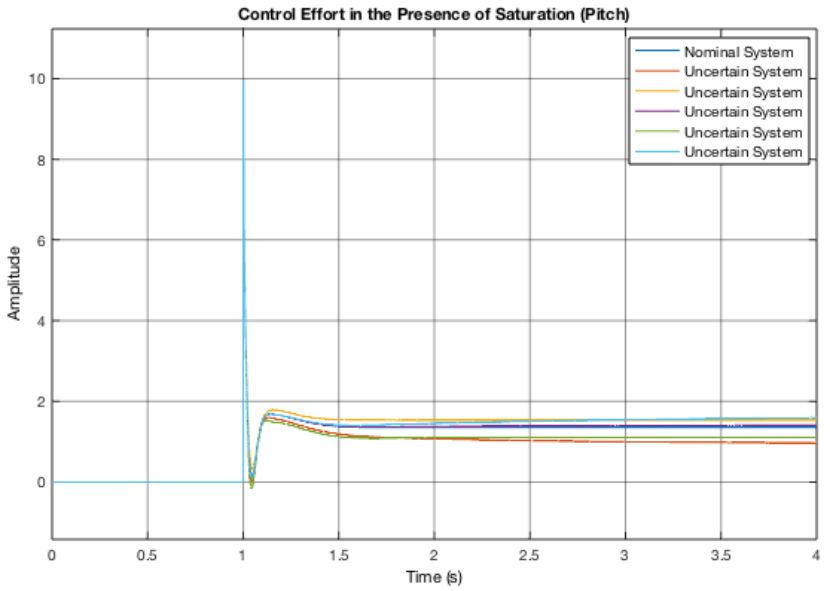

Figure 3.18. Control Effort Signal in the Presence of Saturation (Pitch)

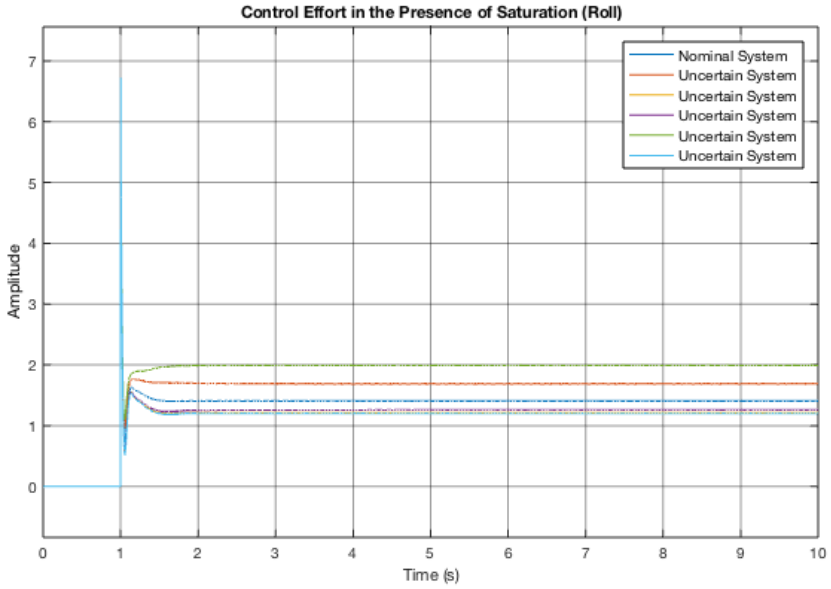

Figure 3.19. Control Effort Signal in the Presence of Saturation (Roll)

3.7. Testing in the Presence of Disturbance and Noise

It is essential to test the robustness of the system against common disturbances and noise. Below are standard inputs used to model control effort disturbances, output disturbances, and feedback sensor noise.

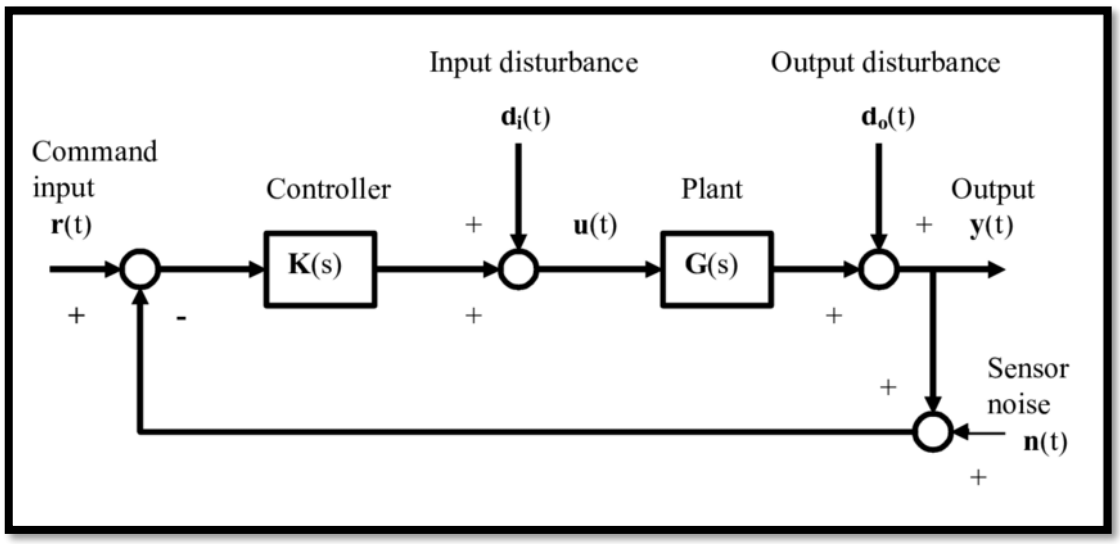

Figure 3.20. Standard Block Diagram with Noise and Disturbance

- Control Effort (Input) Disturbance: Band-Limited White Noise with the Noise Power of 0.001
- Output Disturbance: Pulse Input with the amplitude of 0.1 and period time of 1.5 seconds

- Feedback Noise: The same Band-Limited White Noise to the feedback path

The disturbed systems are also simulated considering saturation in Simulink as shown in the following.

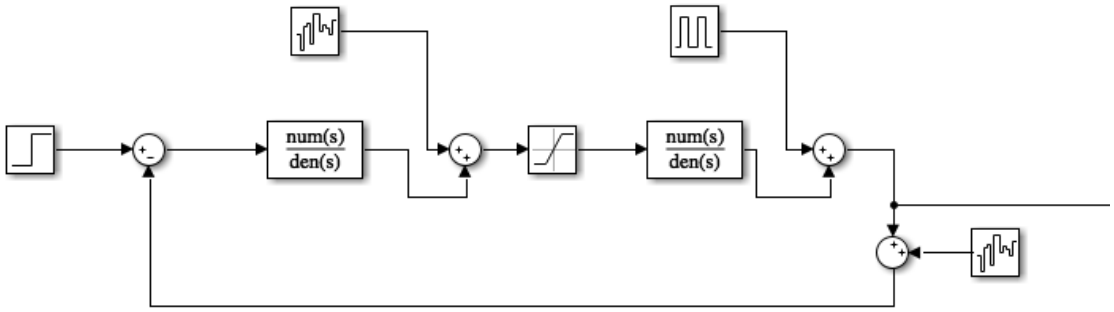

Figure 3.21. Simulation using Simulink in the Presence of Disturbance and Noise

The results validate relative robustness in practical scenarios. Despite noise and dynamic variation, system performance degrades gracefully, and closed-loop stability is preserved.

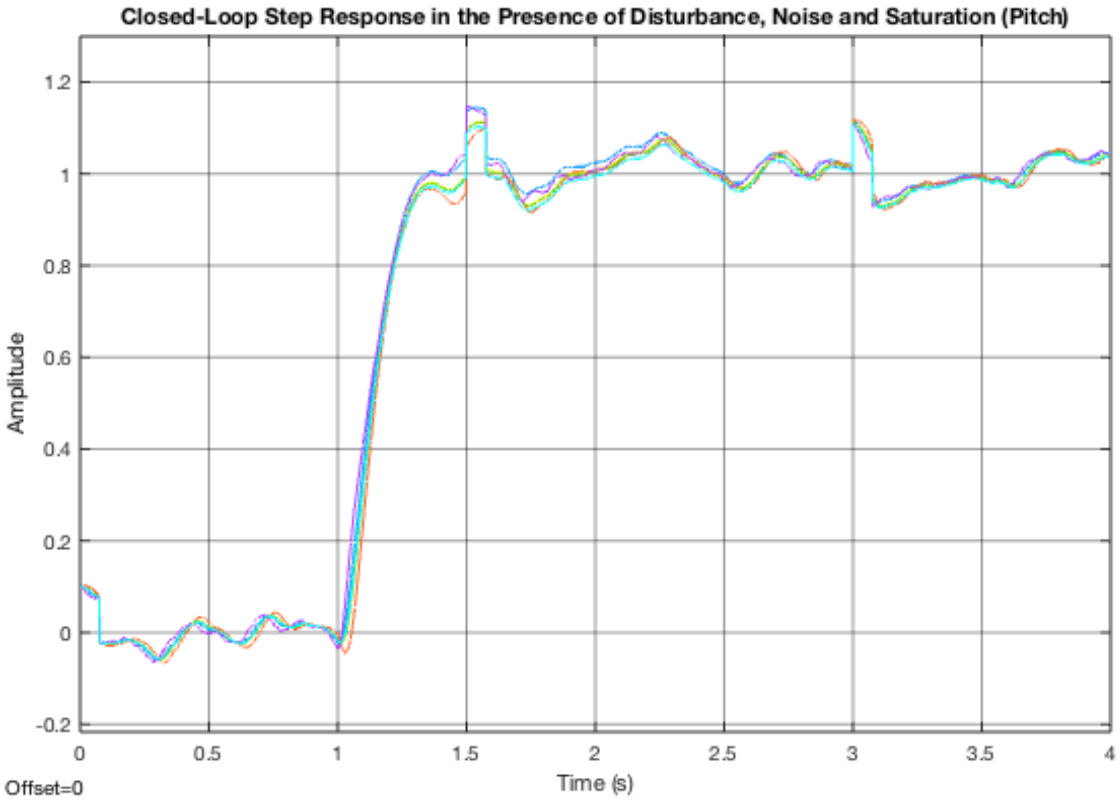

Figure 3.22. Closed-Loop Step Response in the Presence of Undesired Inputs (Pitch)

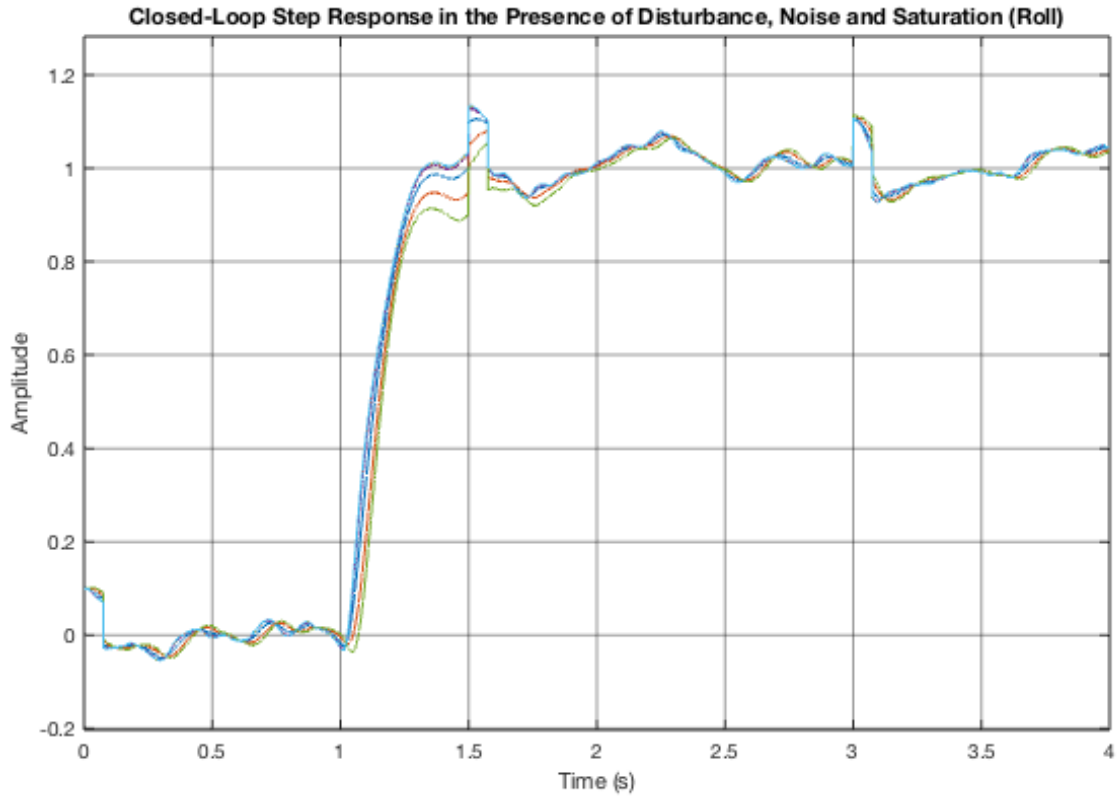

Figure 3.23. Closed-Loop Step Response in the Presence of Undesired Inputs (Roll)

It is possible to neutralize these effects to some extent, however, considering the functional objectives and performance of the system, it is necessary to reduce the noise input as much as possible. It should be noted that the controllers are better at attenuating the disturbance.

4. μ-Synthesis-Based Controller Design

The structured singular value, denoted by μ, quantifies the smallest amount of structured uncertainty that can destabilize a system or cause unacceptable performance degradation. Given a complex matrix M and a structured uncertainty set Δ, the structured singular value μΔ(M) is defined as:

$$\mu_{\Delta}(M) = \frac{1}{\min\{\sigma_{max}(\Delta) \mid \det(I - M\Delta) = 0\}}$$

(I−MΔ) = 0: indicates that the interconnection between M and Δ leads to an unstable or undefined system.

4.1. Robust Stability μ vs. Robust Performance μ

In robust control, structured singular value analysis is used to assess two key properties of a system under uncertainty: robust stability and robust performance. Although both use the same underlying mathematical tool — the structured singular value μ — they differ in their objectives, formulations, and the part of the system they evaluate.

4.2. Robust Stability (μ stab)

Verify whether the closed-loop system remains stable for all admissible uncertainties Δ within a given structure.

$$\mu_{stab}\left(M_{11}(j\omega)\right) < 1 \quad \text{for all } \omega \in R$$

M11 is the submatrix of the full interconnection matrix M, mapping uncertainty inputs to uncertainty outputs.

If the above condition is satisfied, then no structured perturbation Δ with $\|\Delta\|_\infty \leq 1$ can destabilize the system. A peak in μstab close to 1 suggests small robustness margins, meaning the system is near instability.

First, we analyze the robust stability of both θ and φ channels. As observed, the μ value for both θ and φ remains below 1, indicating robust stability.

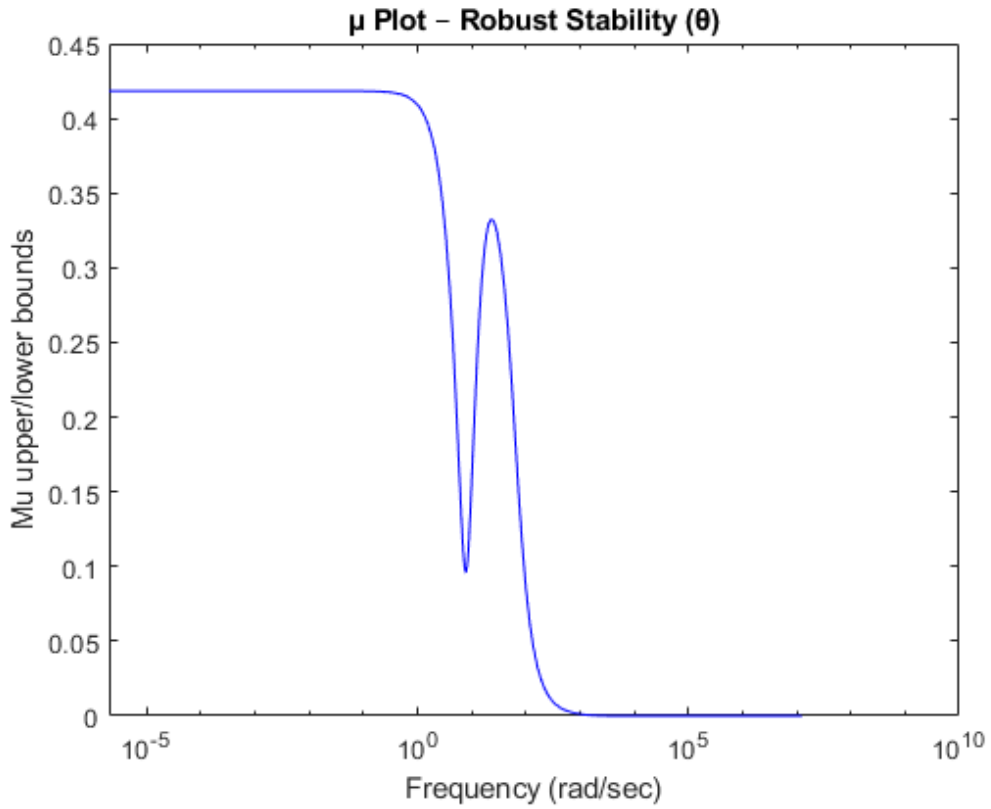

Figure 4.1. Robust Stability of tetha

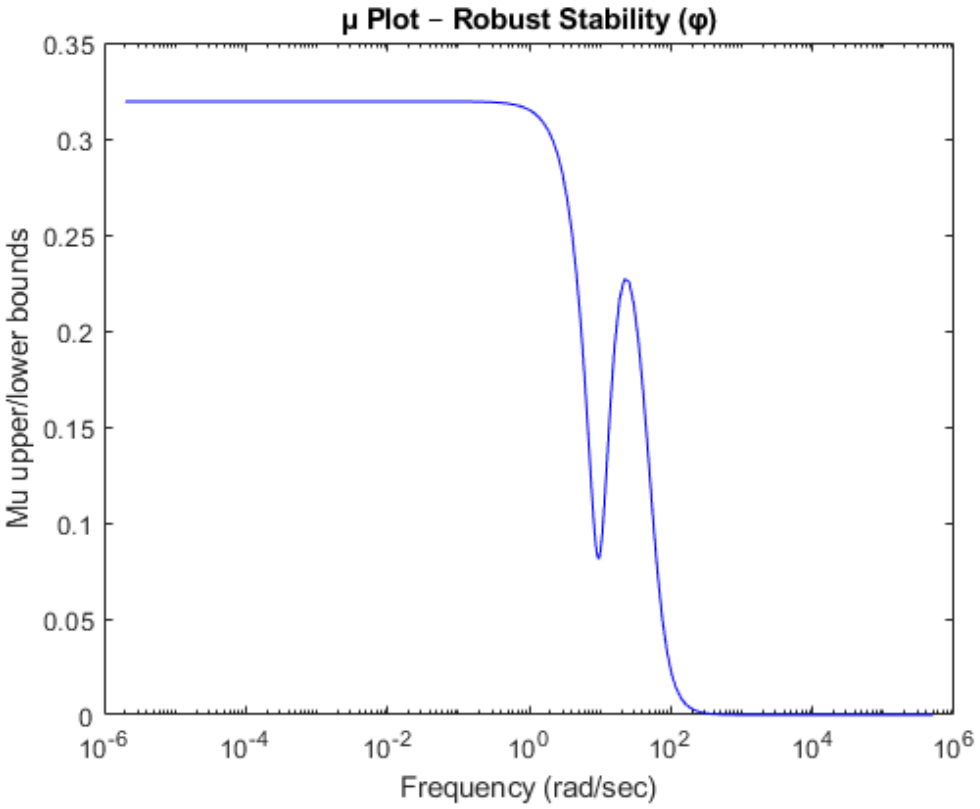

Figure 4.2. Robust Stability of phi angle

4.3. Robust Performance μ_{perf}

Ensure the system maintains acceptable performance (e.g., disturbance rejection, tracking, noise attenuation) despite the presence of structured uncertainties.

$$\mu_{perf}\big(M(j\omega)\big) < 1 \quad \text{for all } \omega \in R$$

M is the full augmented interconnection matrix that includes both the uncertainty paths and performance channels.

If the condition μ_{perf} <1 holds across all frequencies, the system meets the specified performance requirements despite the presence of structured uncertainties. However, if μ exceeds 1 at any frequency, it indicates that the performance specification is violated under some allowable uncertainty at that frequency, revealing sensitivity to uncertainty and a lack of robust performance. In other words, the weighted performance norm is **violated**, and there exists at least one uncertainty configuration that causes the system to underperform.

Now we analyze the μ-performance of both the θ and φ channels. As observed, the μ value exceeds 1 for both cases, indicating that the closed-loop systems may not meet the desired performance specifications under the given structured uncertainties.

Therefore, based on the μ-analysis of the closed-loop systems, it can be concluded that an H∞ controller does not always guarantee robust performance in the presence of structured uncertainties.

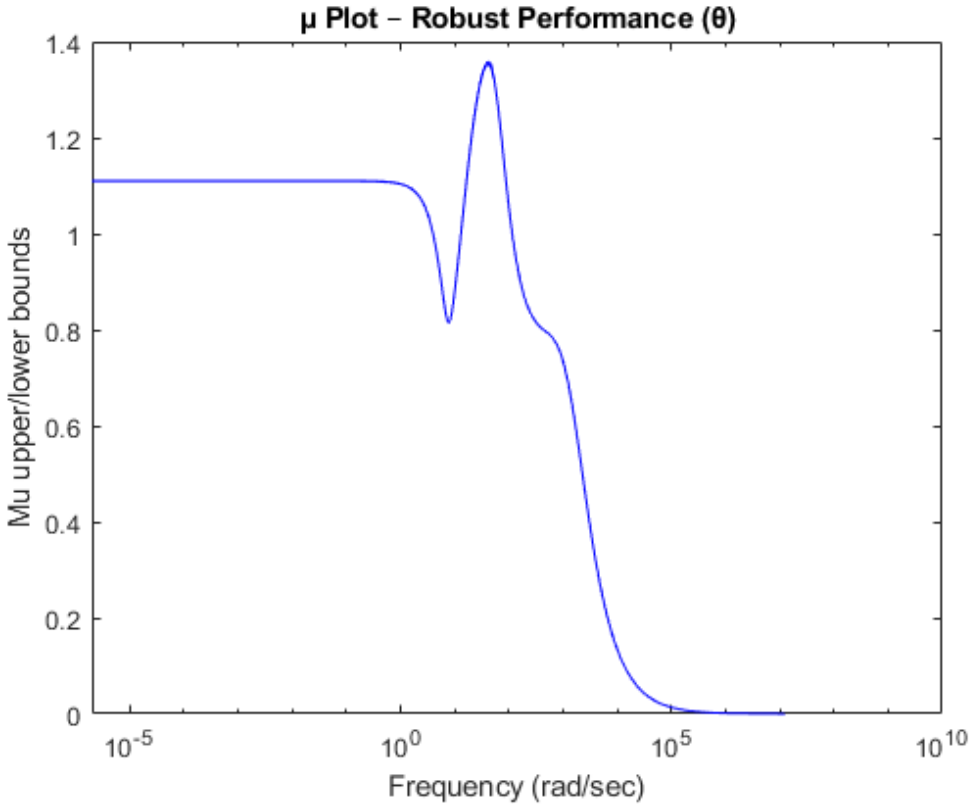

Figure 4.3. Robust Performance of tetha angle

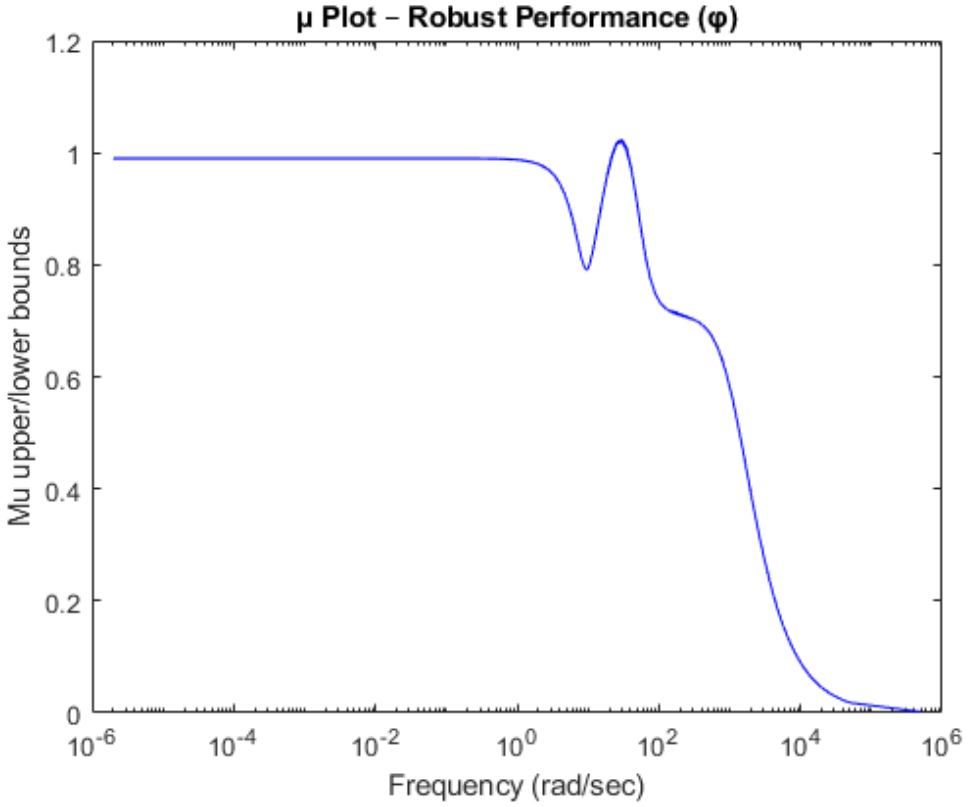

Figure 4.4.Robust Performance of phi angle

- **Possible Cause**

Overly Stringent Performance Requirements The performance weight may demand very small sensitivity (high disturbance rejection or tracking accuracy) at frequencies where it's physically or practically unattainable — particularly if:

$$W_s(j\omega) \text{ is too large for some}$$

- **Remedies**

Adjust the Performance Weight $W\ P$ to bring $\mu_{\text{perf}} < 1$, you can relax the performance specifications by modifying $W\ P$: Reduce the magnitude of W P(s) at frequencies where $\mu_{\text{perf}}(j\omega)$ exceeds 1. This implies that you are tolerating more error (i.e., larger sensitivity) at those frequencies, making the performance requirement less strict and thus easier to satisfy in the presence of uncertainty.

To address the high μ-performance in the θ channel (which reaches approximately 1.4), we reduced the gain of the performance weighting function Ws ,by setting its scaling factor to 1. Subsequently, for both θ and φ channels, we applied the D-K iteration method to further reduce the μ-performance to below 1.

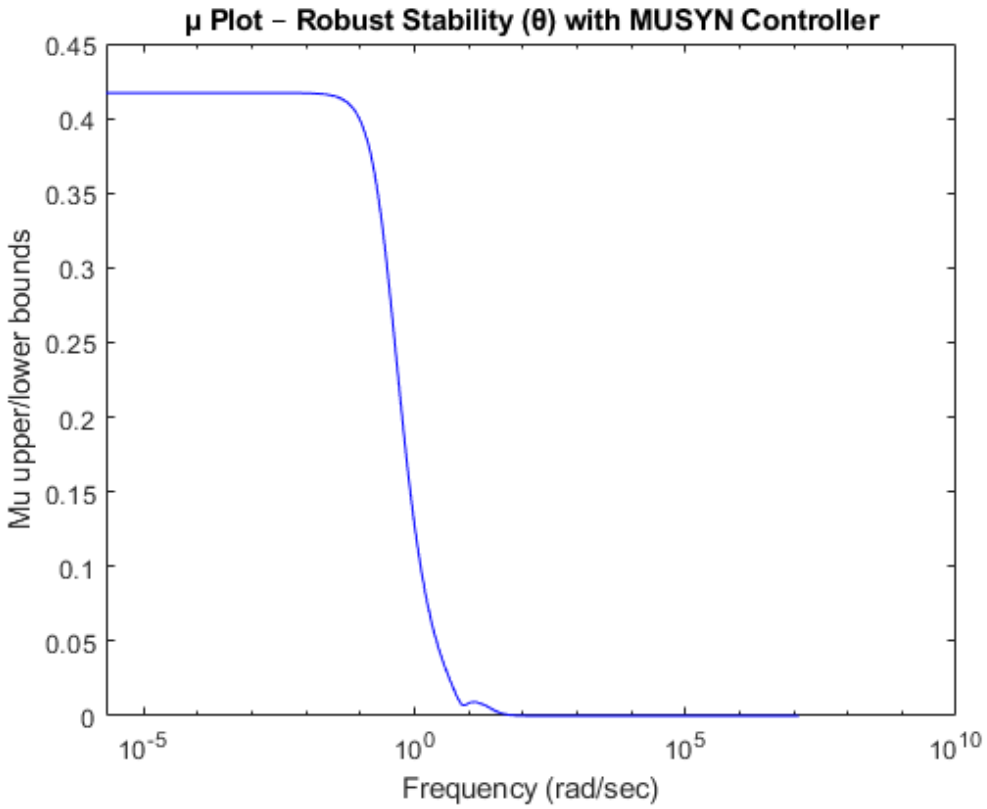

Figure 4.5. Robust Stability with MUSYN Controller for tetha angle

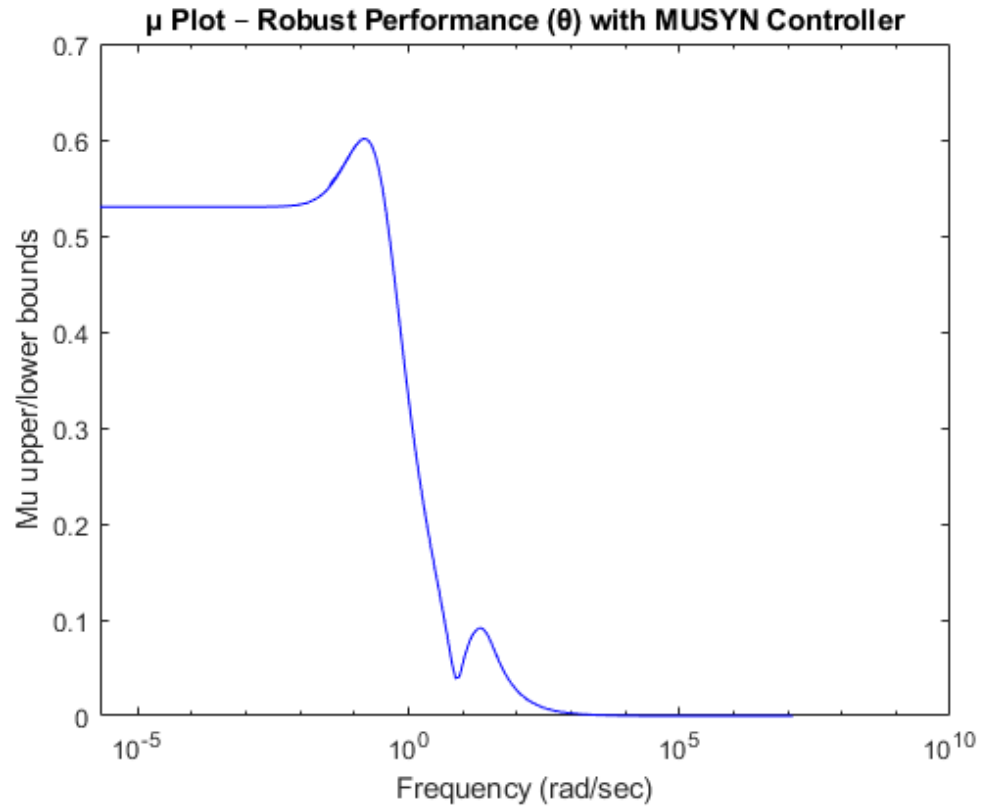

Figure 4.6. Robust performance with MUSYN Controller for tetha angleR

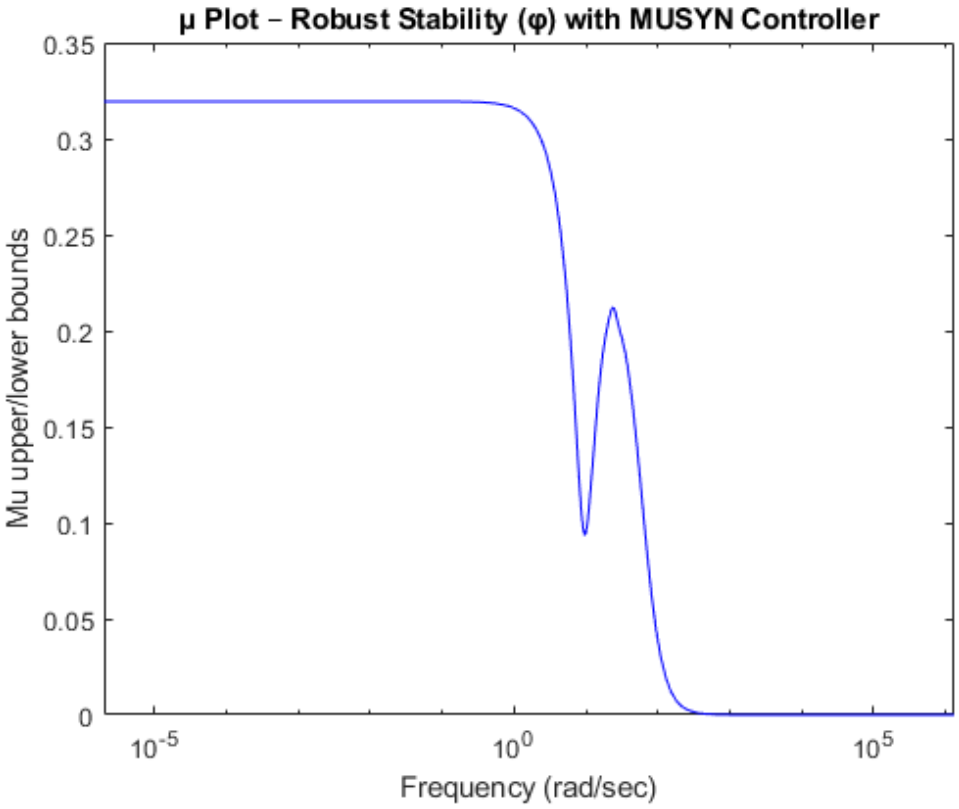

Figure 4.7. Robust Stability with MUSYN Controller for phi angle

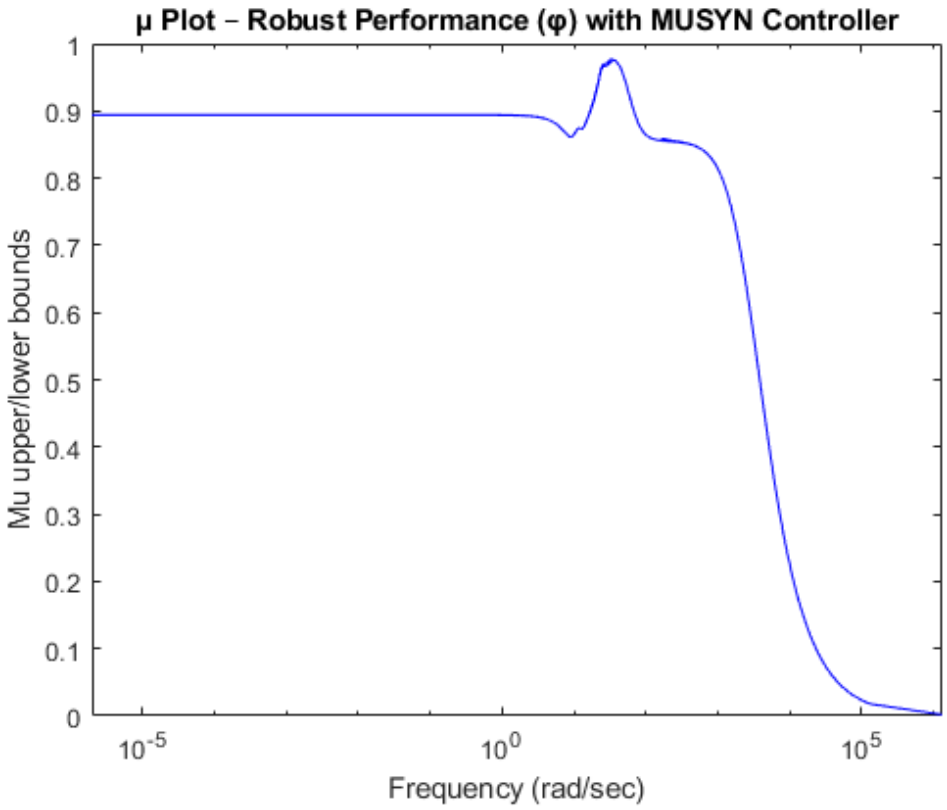

Figure 4.8. Robust performance with MUSYN Controller for phi angle

At this stage, the μ-performance for both θ and φ channels has been successfully reduced to below 1. As observed, the transfer function of the θ channel has a degree of 8 in both the H∞ and μ-synthesis methods. For the φ channel, the transfer function obtained using the H∞ method has a degree of 8, while the one from the μ-synthesis method has a significantly higher degree of 26. Therefore, model order reduction such as the Hankel-based method is required to obtain a lower-order approximation suitable for practical implementation.

$$C_{\mathrm{musyn}_\theta}(s)$$

$$= \frac{0.9985s^7 + 2.578 \times 10^4 s^6 + 2.607 \times 10^7 s^5 + 1.315 \times 10^9 s^4 + 3.189 \times 10^{10} s^3 + 5.557 \times 10^{11} s^2 + 4}{s^8 + 2.584 \times 10^4 s^7 + 2.646 \times 10^7 s^6 + 1.678 \times 10^9 s^5 + 5.228 \times 10^{10} s^4 + 8.877 \times 10^{11} s^3 + 6.458 \times 10^{12} s}$$

$$C_{\mathrm{musyn}_\phi}(s)$$

$$= \frac{4.449 \times 10^4 s^{25} + 8.239 \times 10^7 s^{24} + 5.9 \times 10^{10} s^{23} + 2.129 \times 10^{13} s^{22} + 4.324 \times 10^{15} s^{21} + 5475 \times s^{20} +}{s^{26} + 4880 s^{25} + 7.809 \times 10^6 s^{24} + 5.727 \times 10^9 s^{23} + 2.248 \times 10^{12} s^{22} + 5.209 \times 10^{14} s^{21} + 7.805 \times 10^{16} s^2}$$

We applied the Hankel method for model order reduction. First, we reduced the controller to a third-order system; however, as shown in the frequency response plot, it could not accurately follow the original controller. When we increased the reduced order to 5, the approximation closely matched the original controller's behavior.

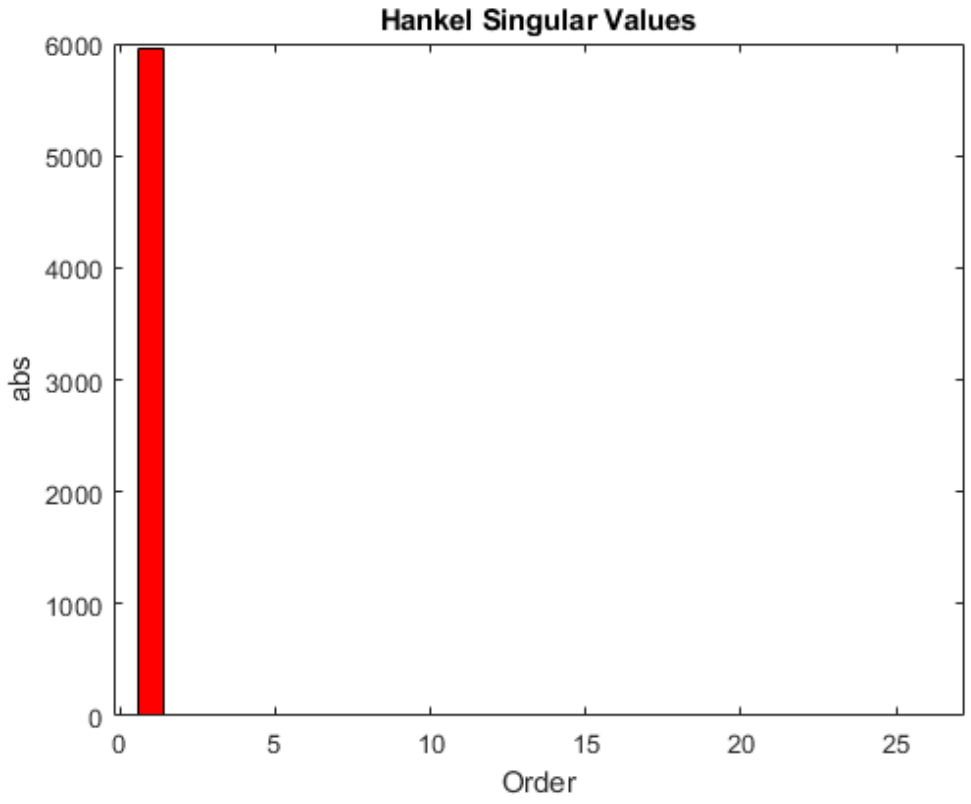

Figure 4.9 : Hankle Singular Values

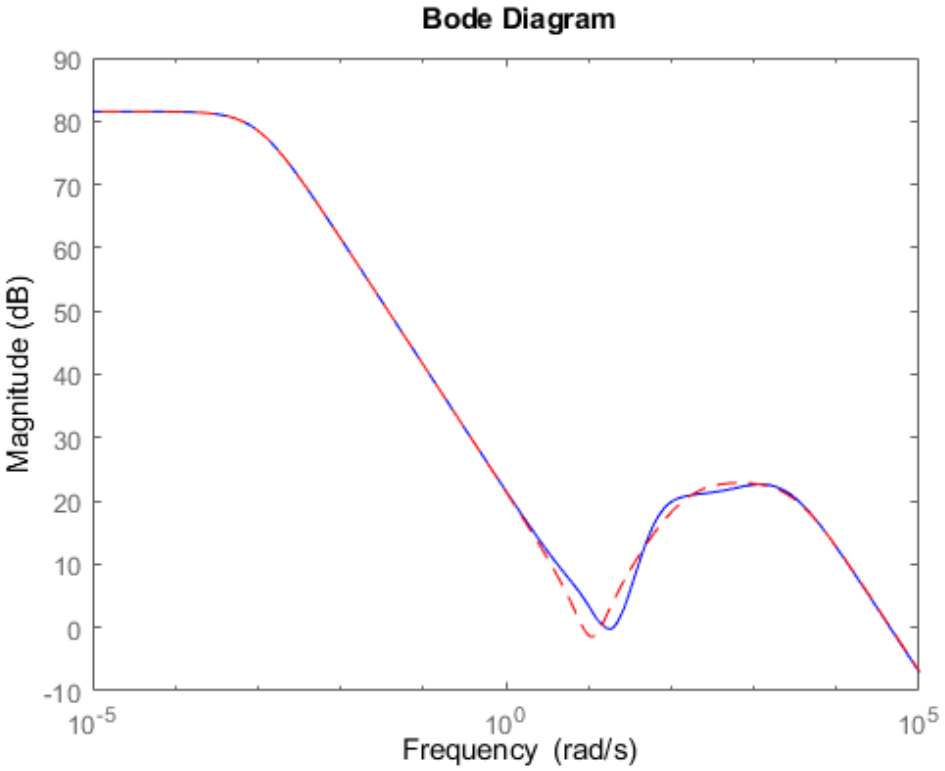

Figure 4.10. Bode Diagram when degree of reduce is 3

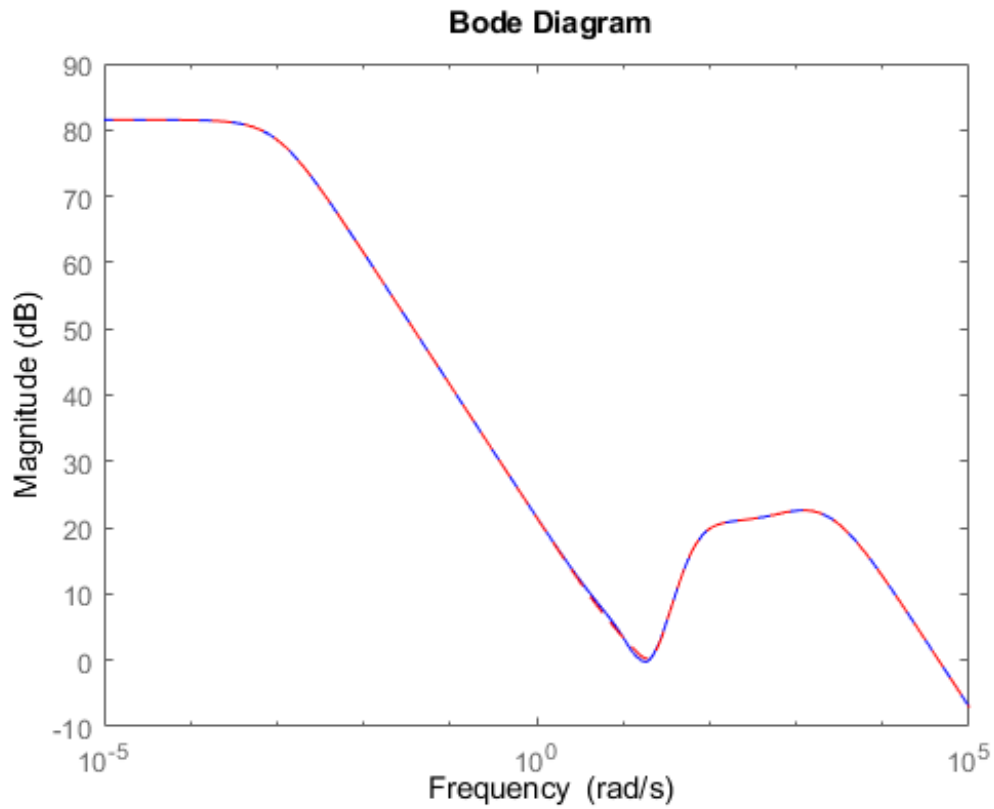

Figure4.11. Bode Diagram of when degee of reduce is 5.

$$C_{\text{musyn}_\phi}^{\text{reduced}}(s)$$

$$= \frac{4.449 \times 10^4 s^4 + 3.062 \times 10^7 s^3 + 8.69 \times 10^8 s^2 + 2.019 \times 10^{10} s + 1.453 \times 10^{11}}{s^5 + 3716 s^4 + 2.98 \times 10^6 s^3 + 2.73 \times 10^8 s^2 + 1.218 \times 10^{10} s + 1.218 \times 10^7}$$

The results are shown in the following two figures. For the θ output, the μ-synthesis controller reduces noise and oscillations effectively. However, due to the difference in the weighting function Ws compared to the H∞ design, the system exhibits a longer rise time and settling time.

In contrast, for the φ output, since the same Ws is used in both methods and only the synthesis technique is changed (from H∞ to μ-synthesis), the rise time and settling time remain similar. The μ-synthesis method mainly makes the transient response slightly more oscillatory without significant improvements in speed.

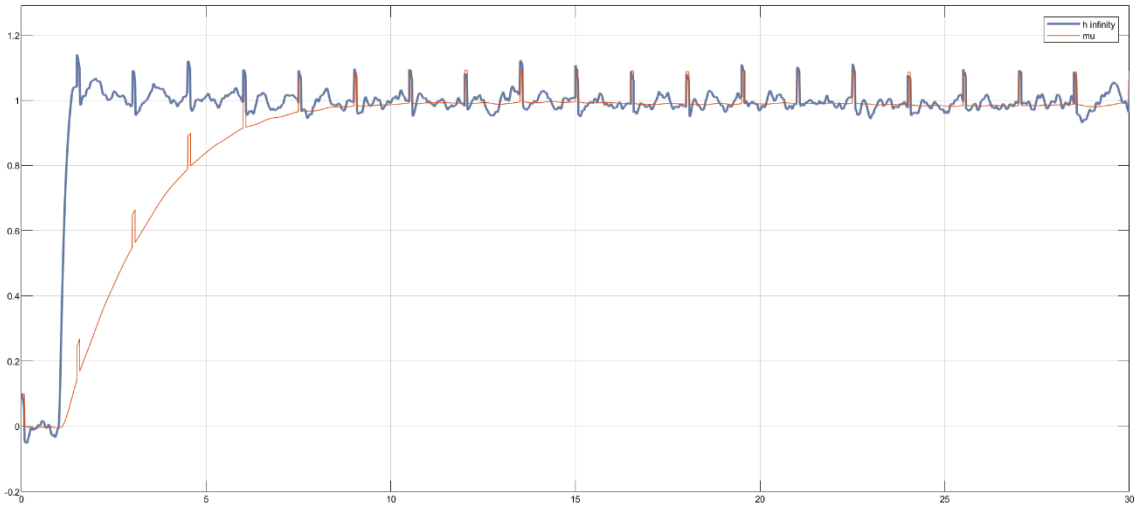

Figure 0.12. tetha Simulation

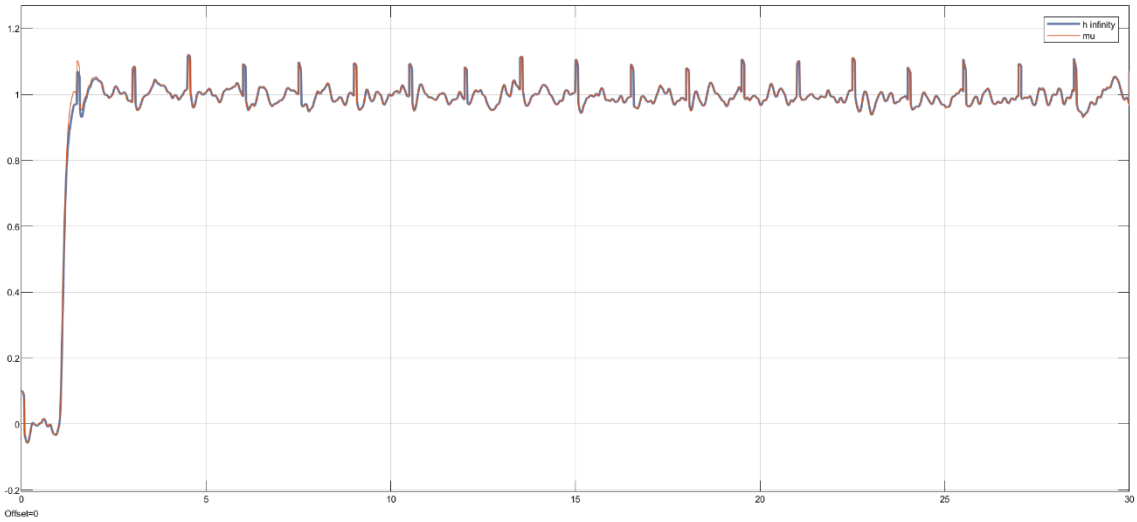

Figure 4.13. Phi simulation

Conclusion

This study illustrates a complete pipeline for robust quadrotor attitude control using both H_∞ and μ-synthesis techniques. Through system identification and multiplicative uncertainty modeling, the controllers are synthesized using mixed-sensitivity criteria and embedded in a cascade architecture. Rigorous simulation tests reveal that H_∞ control yields fast settling times and low overshoot with tractable controller order, making it suitable for many practical applications. In contrast, μ-synthesis offers superior robustness margins and can explicitly handle structured uncertainties but often results in higher-order controllers and more intricate tuning processes. Both methods respect actuator constraints and demonstrate stability under saturation, sensor noise, and external disturbances. By comparing these strategies, the report provides valuable insight into trade-offs between performance, robustness, and complexity in robust control design.

References

[1] Ali Noormohammadi-Asl, Omid Esrafilian, Mojtaba Ahangar Arzati and Hamid D. Taghirad, *"System Identification and H_∞-based Control of Quadrotor Attitude"*, Advanced Robotics and Automated Systems (ARAS), Faculty of Electrical Engineering, K. N. Toosi University of Technology, January 2020.

[2] Hamid D. Taghirad, *"Robust H_∞ Control"*, K. N. Toosi University of Technology, Second Edition, 2024.